

CONSERVATIVE DISCONTINUOUS FINITE VOLUME AND MIXED SCHEMES FOR A NEW FOUR-FIELD FORMULATION IN POROELASTICITY

SARVESH KUMAR¹, RICARDO OYARZÚA^{2,3}, RICARDO RUIZ-BAIER^{4,5,*} AND
RUCHI SANDILYA⁶

Abstract. We introduce a numerical method for the approximation of linear poroelasticity equations, representing the interaction between the non-viscous filtration flow of a fluid and the linear mechanical response of a porous medium. In the proposed formulation, the primary variables in the system are the solid displacement, the fluid pressure, the fluid flux, and the total pressure. A discontinuous finite volume method is designed for the approximation of solid displacement using a dual mesh, whereas a mixed approach is employed to approximate fluid flux and the two pressures. We focus on the stationary case and the resulting discrete problem exhibits a double saddle-point structure. Its solvability and stability are established in terms of bounds (and of norms) that do not depend on the modulus of dilation of the solid. We derive optimal error estimates in suitable norms, for all field variables; and we exemplify the convergence and locking-free properties of this scheme through a series of numerical tests.

Mathematics Subject Classification. 65N30, 76S05, 74F10, 65N15.

Received November 1, 2018. Accepted August 29, 2019.

1. INTRODUCTION

The linear poroelasticity equations constitute one of the simplest continuum models for fluid-structure interaction. In the classical description of the consolidation problem by Biot (see the seminal paper [12]), the filtration of a viscous fluid within the porous skeleton is described by Darcy's law, whereas the deformation of the solid material is governed by Hooke's linear elasticity. The formalism assumes that the porous medium is saturated by the interstitial fluid. Modern applications of this classical framework include numerous problems in science and engineering, where notable examples are logging technologies and the study of borehole instabilities, the behaviour of soils under tunnelling, or in the process of CO₂ sequestration; as well as biomedical investigations

Keywords and phrases. Biot problem, discontinuous finite volume methods, mixed finite elements, locking-free approximations, conservative schemes, error estimates.

¹ Department of Mathematics, Indian Institute of Space Science and Technology, Thiruvananthapuram 695547, Kerala, India.

² GIMNAP, Departamento de Matemática, Universidad del Bío-Bío, Casilla 5-C, Concepción, Chile.

³ Centro de Investigación en Ingeniería Matemática (CI²MA), Universidad de Concepción, Concepción, Chile.

⁴ Mathematical Institute, University of Oxford, Woodstock Road, Oxford OX2 6GG, UK.

⁵ Universidad Adventista de Chile, Casilla 7-D, Chillán, Chile.

⁶ Weierstrass Institute for Applied Analysis and Stochastics, 10117 Berlin, Germany.

*Corresponding author: ruizbaier@maths.ox.ac.uk

such as the characterisation of biological soft tissue (*e.g.* arterial walls, skin, lungs, cardiac muscle, and articular cartilage).

Due to the coupling of flow, transport, and conservation of linear momentum, obtaining analytical solutions for poroelasticity equations is not trivial, and one has therefore to rely on computational simulations. However, the success in accurately replicating poroelasticity solutions using numerical methods is often affected by the manifestation of three unphysical scenarios: spurious pressure modes, locking phenomena (instabilities and polluted convergence of the solid displacement approximation), and loss of mass. In view of remediating these shortcomings encountered in the solutions produced with classical methods and formulations, here we extend the three-field formulation proposed in [39, 47] (where classical finite elements can be employed straightforwardly without the risk of producing the first two spurious phenomena), and we further introduce a family of discontinuous finite volume (DFV) – mixed finite element (MFE) schemes that aim at rectifying the third nonphysical situation. Apart from enabling robustness with respect to the incompressibility limit (at the additional cost of coupling with one scalar equation), the additional unknown of total pressure used here and in [39, 47] has also a clear physical meaning. It encompasses the contributions of isotropic stress from fluid and solid phases, and it constitutes a more natural extension of the so-called Hermann formulation (displacement-pressure) for elasticity, to the case of poromechanics, and it has special interest in some recent extended models such as the so-called multiple-network poroelasticity and the method proposed in [40]. Therein, the authors indicate that using the total pressure has an important quantitative impact on the computation of displacement magnitude for certain tests cases.

With the exception of the finite volume (FV) discretisation of Biot's system applied in [8, 45], the numerical solution of poroelasticity equations has been traditionally associated with finite element (FE) methods. Some of these studies include stabilised conforming schemes for primal formulations and least-squares FE methods [1, 9, 10, 27, 42, 44, 62, 63, 66] (see also the extensive review [41]); as well as HDG schemes [28], DG methods [21, 35, 53] (in particular, conservative schemes from [33, 34, 36]), and HHO methods (hybrid high-order discretisations which are conservative and robust with respect to locking and spurious pressure modes, advanced in [13]). On the other hand, a few schemes that combine discontinuous Galerkin (or finite volume, or weak Galerkin) discretisations and mixed methods solving also for the fluid flux, have been proposed in [19, 50, 55, 59, 65]. Apart from reproducing accurately the mechanical equilibrium, guaranteeing the conservation of fluid mass is of substantial importance in most applications. Some dedicated techniques are available, including for instance the stabilised method in [24]; and the reconstruction of stress and fluid fluxes by a modified Arnold–Winther scheme, recently analysed in [52]. Other double mixed formulations (mixed for the elasticity and mixed for Darcy's flow) have been recently rigorously analysed in [2]. These schemes are particularly useful when fluid flux and stress act as coupling variables with other phenomena such as thermal processes, multiphase flows, or chemical reactions. We also point out that stability and monotonicity issues related to numerical methods for Biot's equations are addressed in [54]. As mentioned above, an important aspect is the robustness of the methods with respect to model parameters. This has been achieved for Biot and multiple network poroelasticity in the very recent works [33, 34]. There the authors are able to derive stability bounds independent of the Lamé constants, but also independence with respect to constrained specific storage and solid permeability. Their results hinge on the definition of parameter-dependent norms for displacement, fluid flux, and fluid pressure. In addition, using the classical framework of abstract Riesz representation of perturbed linear problems developed in [43], they present adequate block preconditioners that preserve parameter robustness.

Here we also aim at developing stable and convergent schemes using similar ideas as those in [40, 47]; but the primary differences with respect to the contributions listed above is that we use a special blend of DFV and MFE methods for the numerical approximation of the underlying coupled problem, recast in terms of solid displacement, fluid flux, fluid pressure, and total pressure. FV schemes are a particular class of Petrov–Galerkin methods that require to define trial and test spaces associated with primal and dual partitions of the domain, respectively. Different types of dual meshes are employed when the FV method is of conforming, non-nonconforming, or discontinuous type (see details and comparisons in *e.g.* [18]), but in most cases they feature local conservativity as well as suitability for deriving energy and L^2 -error estimates. Moreover, schemes

using DFV approximations preserve features of both DG and general FV methods, including smaller support of dual elements (when compared with conforming and non-conforming FV schemes) as well as appropriateness in handling discontinuous coefficients. Establishing the solvability of the continuous formulation and the stability bounds for the proposed numerical schemes in a robust manner is not trivial, since we do not employ parameter-weighted norms as done, *e.g.* [33, 34, 39, 40, 43]. In particular, a current limitation in our approach is that the structure of our analysis does not permit to treat the case of zero constrained specific storage coefficients. However our numerical experiments show that this might be only a technical requirement.

We have structured the contents of this paper as follows. Section 2 outlines the main ingredients of the model problem and carry out its solvability and stability analysis. A family of DFV-MFE methods is then introduced in Section 3, and the invertibility of the discrete solution operator is derived in Section 4. The error analysis of the proposed schemes is addressed next in Section 5, and in Section 6 we provide a few numerical tests illustrating the properties of the proposed method. We close in Section 7 with a summary and discussion of possible extensions.

2. THE GOVERNING EQUATIONS IN A MIXED-MIXED STRUCTURE

2.1. Preliminaries

From now on we will adopt the classical notation for Lebesgue and Sobolev spaces. In addition by \mathbf{M} and \mathbb{M} we will denote the corresponding vectorial and tensorial counterparts of the generic scalar functional space M . For instance, if $\Theta \subseteq \mathbf{R}^d$, $d = 2, 3$ is a domain, $\Lambda \subseteq \mathbf{R}^d$ is a Lipschitz surface, and $r \in \mathbf{R}$, we define $\mathbf{H}^r(\Theta) := [\mathbf{H}^r(\Theta)]^d$ and $\mathbf{H}^r(\Lambda) := [\mathbf{H}^r(\Lambda)]^d$. By $\mathbf{0}$ we will refer to the generic zero vector and we will denote by C and c , with or without subscripts, bars, tildes or hats, generic constants independent of the discretisation parameters. We recall that $\mathbf{H}(\text{div}; \Theta) := \{\boldsymbol{\tau} \in \mathbf{L}^2(\Theta) : \nabla \cdot \boldsymbol{\tau} \in L^2(\Theta)\}$ associated with the norm

$$\|\boldsymbol{\tau}\|_{\text{div}, \Theta}^2 := \|\boldsymbol{\tau}\|_{0, \Theta}^2 + \|\nabla \cdot \boldsymbol{\tau}\|_{0, \Theta}^2,$$

is a Hilbert space.

As a model problem we consider a homogeneous porous medium constituted by a mixture of incompressible grains and interstitial fluid. The domain of interest $\Omega \subset \mathbf{R}^d$, $d = 2, 3$ is assumed bounded and simply connected. For a given body force \mathbf{f} and a given volumetric fluid source ℓ , we will concentrate the discussion on the following four-field mixed-mixed formulation of Biot's equations: find the displacements of the porous skeleton, \mathbf{u} , the total pore pressure of the fluid, p , the fluid flux, $\boldsymbol{\sigma}$, and the total fluid-structure pressure (or total volumetric stress), ϕ ; satisfying

$$-\mathbf{div}(2\mu\boldsymbol{\varepsilon}(\mathbf{u}) - \phi\mathbf{I}) = \mathbf{f} \quad \text{in } \Omega, \quad (2.1)$$

$$\phi = \alpha p - \lambda \mathbf{div} \mathbf{u} \quad \text{in } \Omega, \quad (2.2)$$

$$\boldsymbol{\sigma} = -\frac{\kappa}{\eta}(\nabla p - \rho\mathbf{g}) \quad \text{in } \Omega, \quad (2.3)$$

$$\left(c_0 + \frac{\alpha^2}{\lambda}\right)p - \frac{\alpha}{\lambda}\phi + \mathbf{div} \boldsymbol{\sigma} = \ell \quad \text{in } \Omega, \quad (2.4)$$

where $\boldsymbol{\varepsilon}(\mathbf{u}) = \frac{1}{2}(\nabla \mathbf{u} + \nabla \mathbf{u}^T)$ is the tensor of infinitesimal strains, κ is the permeability of the porous solid (assumed uniformly bounded $0 < \kappa_1 \leq \kappa(\mathbf{x}) \leq \kappa_2 < \infty$, for all $\mathbf{x} \in \Omega$), λ, μ are the Lamé constants of the solid (moduli of dilation and shear, respectively), $c_0 > 0$ is the constrained specific storage coefficient, $\alpha > 0$ is the Biot-Willis parameter, \mathbf{g} is the gravity acceleration; and $\eta > 0, \rho > 0$ are the viscosity and density of the pore fluid. In a stationary setting, equation (2.1) states conservation of momentum for the mixture, (2.4) corresponds to mass conservation of the fluid content (for instance resulting at time iteration when doing a semidiscretisation in time of the transient Biot equations), and (2.2), (2.3) define the new unknowns in the system in terms of the primal variables.

The boundary of Ω is assumed disjointly split into segments or surfaces where Dirichlet conditions are to be considered for fluid pressure and solid displacements: $\partial\Omega = \bar{\Gamma}_p \cup \bar{\Gamma}_u$, $\Gamma_p \cap \Gamma_u = \emptyset$. These prescriptions are accompanied by zero normal total stress, and by zero normal fluid flux, respectively. In summary, we endow the system (2.1)–(2.4) with the following boundary conditions

$$p = p_\Gamma, \quad (2\mu\varepsilon(\mathbf{u}) - \phi\mathbf{I})\mathbf{n} = \mathbf{0} \text{ on } \Gamma_p, \quad \text{and} \quad \mathbf{u} = \mathbf{0}, \quad \boldsymbol{\sigma} \cdot \mathbf{n} = 0 \text{ on } \Gamma_u, \quad (2.5)$$

where \mathbf{n} is the exterior unit normal vector on $\partial\Omega$ and $p_\Gamma \in H_{00}^{1/2}(\Gamma_p) := \{v|_{\Gamma_p} : v \in H_{\Gamma_u}^1(\Omega)\}$, with $H_{\Gamma_u}^1(\Omega) := \{v \in H^1(\Omega) : v|_{\Gamma_u} = 0\}$. The space $H_{00}^{1/2}(\Gamma_p)$ is endowed with the norm

$$\|\xi\|_{1/2,00,\Gamma_p} := \inf\{\|v\|_{1,\Omega} : v \in H_{\Gamma_u}^1(\Omega) \text{ and } v|_{\Gamma_p} = \xi\}.$$

More elaborated boundary conditions can be found in *e.g.* [57].

2.2. Weak formulation

We proceed to test equations (2.1)–(2.4) against appropriate functions and to integrate by parts. This step leads to the following weak formulation of the coupled problem: find $\mathbf{u} \in \mathbf{H}$, $\phi \in Q$, $\boldsymbol{\sigma} \in \mathbf{Z}$, and $p \in Q$ such that

$$a_s(\mathbf{u}, \mathbf{v}) + b_s(\mathbf{v}, \phi) = F(\mathbf{v}) \quad \forall \mathbf{v} \in \mathbf{H}, \quad (2.6)$$

$$b_s(\mathbf{u}, \psi) - c_s(\phi, \psi) + b_{sf}(\psi, p) = 0 \quad \forall \psi \in Q, \quad (2.7)$$

$$a_f(\boldsymbol{\sigma}, \boldsymbol{\tau}) + b_f(\boldsymbol{\tau}, p) = G(\boldsymbol{\tau}) \quad \forall \boldsymbol{\tau} \in \mathbf{Z}, \quad (2.8)$$

$$b_{sf}(\phi, q) + b_f(\boldsymbol{\sigma}, q) - c_f(p, q) = H(q) \quad \forall q \in Q, \quad (2.9)$$

where the bilinear forms and linear functionals appearing in (2.6)–(2.9) (denoted with a subscript s or f whenever the arguments are solely related to structure or to fluid variables, respectively) are specified in the following way

$$\begin{aligned} a_s(\mathbf{u}, \mathbf{v}) &:= 2\mu \int_{\Omega} \varepsilon(\mathbf{u}) : \varepsilon(\mathbf{v}), \quad b_s(\mathbf{v}, \psi) := - \int_{\Omega} \psi \operatorname{div} \mathbf{v}, \quad b_{sf}(\psi, q) := \frac{\alpha}{\lambda} \int_{\Omega} \psi q, \quad c_s(\phi, \psi) := \frac{1}{\lambda} \int_{\Omega} \phi \psi, \\ a_f(\boldsymbol{\sigma}, \boldsymbol{\tau}) &:= \frac{\eta}{\kappa} \int_{\Omega} \boldsymbol{\sigma} \cdot \boldsymbol{\tau}, \quad b_f(\boldsymbol{\tau}, q) := - \int_{\Omega} q \operatorname{div} \boldsymbol{\tau}, \quad c_f(p, q) := \left(c_0 + \frac{\alpha^2}{\lambda} \right) \int_{\Omega} p q, \\ F(\mathbf{v}) &:= \int_{\Omega} \mathbf{f} \cdot \mathbf{v}, \quad G(\boldsymbol{\tau}) := \int_{\Omega} \rho \mathbf{g} \cdot \boldsymbol{\tau} - \langle \boldsymbol{\tau} \cdot \mathbf{n}, p_\Gamma \rangle_{\Gamma_p}, \quad H(q) := - \int_{\Omega} \ell q, \end{aligned} \quad (2.10)$$

and the conditions in (2.5) imply that the functional spaces may be chosen as

$$\mathbf{H} := \mathbf{H}_{\Gamma_u}^1(\Omega) = \{\mathbf{v} \in \mathbf{H}^1(\Omega) : \mathbf{v}|_{\Gamma_u} = \mathbf{0}\}, \quad Q := L^2(\Omega), \quad \mathbf{Z} := \{\boldsymbol{\tau} \in \mathbf{H}(\operatorname{div}; \Omega) : \boldsymbol{\tau} \cdot \mathbf{n} = 0 \text{ on } \Gamma_u\}.$$

Notice that the mixed character of the fluid conservation equation implies that the Dirichlet datum for the fluid pressure appears in the linear functional G .

2.3. Properties of the involved forms

Thanks to the Cauchy–Schwarz inequality, it is readily seen that all bilinear forms and linear functionals are uniformly bounded, that is

$$\begin{aligned} |a_s(\mathbf{u}, \mathbf{v})| &\leq 2\mu C_{k,2} \|\mathbf{u}\|_{1,\Omega} \|\mathbf{v}\|_{1,\Omega}, \quad |a_f(\boldsymbol{\sigma}, \boldsymbol{\tau})| \leq \frac{\eta}{\kappa_1} \|\boldsymbol{\sigma}\|_{\operatorname{div}, \Omega} \|\boldsymbol{\tau}\|_{\operatorname{div}, \Omega}, \\ |b_s(\mathbf{v}, \psi)| &\leq \|\mathbf{v}\|_{1,\Omega} \|\psi\|_{0,\Omega}, \quad |b_{sf}(\psi, q)| \leq \alpha \lambda^{-1} \|\psi\|_{0,\Omega} \|q\|_{0,\Omega}, \quad |b_f(\boldsymbol{\tau}, q)| \leq \|\boldsymbol{\tau}\|_{\operatorname{div}, \Omega} \|q\|_{0,\Omega}, \\ |c_s(\phi, \psi)| &\leq \lambda^{-1} \|\phi\|_{0,\Omega} \|\psi\|_{0,\Omega}, \quad |c_f(p, q)| \leq \left(c_0 + \frac{\alpha^2}{\lambda} \right) \|p\|_{0,\Omega} \|q\|_{0,\Omega}, \end{aligned} \quad (2.11)$$

and

$$|F(\mathbf{v})| \leq \|\mathbf{f}\|_{0,\Omega} \|\mathbf{v}\|_{1,\Omega}, \quad |G(\boldsymbol{\tau})| \leq (\rho \|\mathbf{g}\|_{0,\Omega} + \|p_\Gamma\|_{1/2,00,\Gamma_p}) \|\boldsymbol{\tau}\|_{\text{div},\Omega}, \quad |H(q)| \leq \|\ell\|_{0,\Omega} \|q\|_{0,\Omega}, \quad (2.12)$$

for all $\mathbf{u}, \mathbf{v} \in \mathbf{H}$, $p, q, \phi, \psi \in Q$, $\boldsymbol{\sigma}, \boldsymbol{\tau} \in \mathbf{Z}$. Above, $C_{k,2}$ is one of the positive constants satisfying

$$C_{k,1} \|\mathbf{v}\|_{1,\Omega}^2 \leq \|\boldsymbol{\varepsilon}(\mathbf{v})\|_{0,\Omega}^2 \leq C_{k,2} \|\mathbf{v}\|_{1,\Omega}^2, \quad \forall \mathbf{v} \in \mathbf{H}. \quad (2.13)$$

Regarding the positivity of the forms a_s and a_f , we begin by using (2.13), to obtain

$$a_s(\mathbf{v}, \mathbf{v}) \geq 2\mu C_{k,1} \|\mathbf{v}\|_{1,\Omega}^2, \quad \forall \mathbf{v} \in \mathbf{H}. \quad (2.14)$$

In turn, we define

$$K_f := \{\boldsymbol{\tau} \in \mathbf{Z} : b_f(\boldsymbol{\tau}, q) = 0 \quad \forall q \in Q\} = \{\boldsymbol{\tau} \in \mathbf{Z} : \text{div } \boldsymbol{\tau} = 0 \quad \text{in } \Omega\},$$

and observe that the following inequality holds

$$a_f(\boldsymbol{\tau}, \boldsymbol{\tau}) \geq \frac{\eta}{\kappa_2} \|\boldsymbol{\tau}\|_{\text{div},\Omega}^2, \quad \forall \boldsymbol{\tau} \in K_f. \quad (2.15)$$

Finally, we recall the following inf-sup conditions satisfied by the forms b_s and b_f (see *e.g.* [31]):

$$\sup_{\mathbf{v} \in \mathbf{H} \setminus \mathbf{0}} \frac{b_s(\mathbf{v}, \psi)}{\|\mathbf{v}\|_{1,\Omega}} \geq \beta_s \|\psi\|_{0,\Omega} \quad \forall \psi \in Q \quad \text{and} \quad \sup_{\boldsymbol{\tau} \in \mathbf{Z} \setminus \mathbf{0}} \frac{b_f(\boldsymbol{\tau}, q)}{\|\boldsymbol{\tau}\|_{\text{div},\Omega}} \geq \beta_f \|q\|_{0,\Omega} \quad \forall q \in Q, \quad (2.16)$$

with $\beta_s, \beta_f > 0$ depending on $|\Omega|$.

2.4. Analysis of the continuous problem

In what follows we establish the well-posedness and stability of our formulation. To that end we derive the continuous dependence result for (2.6)–(2.9) by considering generic functionals appearing on the corresponding right-hand side. Then, recalling that the problem is defined by a self-adjoint operator from a Hilbert space into itself, the well-posedness and stability can be readily derived (see for instance [15], Cor. 2.18). In addition, we observe in advance that the discrete version of the following theorem, whose proof can be obtained by following the same steps provided next, is crucial for the derivation of a companion error estimate. Let us then define $F_1 \in \mathbf{H}'$, $G_1 \in Q'$, $F_2 \in \mathbf{Z}'$ and $G_2 \in Q'$ and let $(\mathbf{u}, \phi, \boldsymbol{\sigma}, p) \in \mathbf{H} \times Q \times \mathbf{Z} \times Q$, be such that

$$a_s(\mathbf{u}, \mathbf{v}) + b_s(\mathbf{v}, \phi) = F_1(\mathbf{v}) \quad \forall \mathbf{v} \in \mathbf{H}, \quad (2.17)$$

$$b_s(\mathbf{u}, \psi) - c_s(\phi, \psi) + b_{sf}(\psi, p) = G_1(\psi) \quad \forall \psi \in Q, \quad (2.18)$$

$$a_f(\boldsymbol{\sigma}, \boldsymbol{\tau}) + b_f(\boldsymbol{\tau}, p) = F_2(\boldsymbol{\tau}) \quad \forall \boldsymbol{\tau} \in \mathbf{Z}, \quad (2.19)$$

$$b_{sf}(\phi, q) + b_f(\boldsymbol{\sigma}, q) - c_f(p, q) = G_2(q) \quad \forall q \in Q. \quad (2.20)$$

For the subsequent analysis we will appeal to a collection of preliminary results and definitions. We begin by observing that each $\boldsymbol{\tau}$ in \mathbf{Z} can be uniquely decomposed into the form

$$\boldsymbol{\tau} = \boldsymbol{\tau}_0 + \boldsymbol{\tau}^\perp, \quad \text{with } \boldsymbol{\tau}_0 \in K_f \text{ and } \boldsymbol{\tau}^\perp \in K_f^\perp.$$

Then, we define $F_2^0 \in K_f'$ and $F_2^\perp \in (K_f^\perp)'$ be such that

$$F_2(\boldsymbol{\tau}) = F_2^0(\boldsymbol{\tau}_0) + F_2^\perp(\boldsymbol{\tau}^\perp) \quad \forall \boldsymbol{\tau} = \boldsymbol{\tau}_0 + \boldsymbol{\tau}^\perp \in \mathbf{Z}. \quad (2.21)$$

Clearly

$$F_2|_{K_f}(\boldsymbol{\tau}) = F_2^0(\boldsymbol{\tau}_0), \quad F_2|_{K_f^\perp}(\boldsymbol{\tau}) = F_2^\perp(\boldsymbol{\tau}^\perp), \quad F_2^0(\boldsymbol{\tau}^\perp) = 0 \quad \text{and} \quad F_2^\perp(\boldsymbol{\tau}_0) = 0. \quad (2.22)$$

Similarly, we define

$$K_s := \{\mathbf{v} \in \mathbf{H} : b_s(\mathbf{v}, \psi) = 0 \quad \forall \psi \in Q\},$$

and observe that each \mathbf{v} in \mathbf{H} can be uniquely decomposed into the form

$$\mathbf{v} = \mathbf{v}_0 + \mathbf{v}^\perp, \text{ with } \mathbf{v}_0 \in K_s \text{ and } \mathbf{v}^\perp \in K_s^\perp.$$

Let us now observe that from the inf-sup conditions (2.16), there holds

$$\sup_{(\mathbf{v}, \boldsymbol{\tau}) \in (\mathbf{H} \times \mathbf{Z}) \setminus \mathbf{0}} \frac{b_s(\mathbf{v}, \psi) + b_f(\boldsymbol{\tau}, q)}{\|\mathbf{v}\|_{1,\Omega} + \|\boldsymbol{\tau}\|_{\text{div},\Omega}} \geq \beta(\|\psi\|_{0,\Omega} + \|q\|_{0,\Omega}) \quad \forall \psi, q \in Q, \quad (2.23)$$

with $\beta > 0$ independent of λ . From (2.23) and Lemma 2.1 of [29] it can be easily deduced that

$$\sup_{(\psi, q) \in (Q \times Q) \setminus \mathbf{0}} \frac{b_s(\mathbf{v}^\perp, \psi) + b_f(\boldsymbol{\tau}^\perp, q)}{\|\psi\|_{0,\Omega} + \|q\|_{0,\Omega}} \geq \beta(\|\mathbf{v}^\perp\|_{1,\Omega} + \|\boldsymbol{\tau}^\perp\|_{\text{div},\Omega}) \quad \forall (\mathbf{v}^\perp, \boldsymbol{\tau}^\perp) \in K_s^\perp \times K_f^\perp. \quad (2.24)$$

To conclude we define

$$\begin{aligned} C((\phi, p), (\psi, q)) &:= c_s(\phi, \psi) + c_f(p, q) - b_{sf}(\phi, q) - b_{sf}(\psi, p) \\ &= \frac{1}{\lambda} \int_{\Omega} (\phi - \alpha p)(\psi - \alpha q) + c_0 \int_{\Omega} pq, \quad \forall \phi, \psi, p, q \in Q, \end{aligned}$$

and notice that

$$\begin{aligned} |C((\phi, p), (\psi, q))| &\leq C((\phi, p), (\phi, p))^{1/2} (C((\psi, q), (\psi, q)))^{1/2} \\ &= \left(\frac{1}{\lambda} \|\phi - \alpha p\|_{0,\Omega}^2 + c_0 \|p\|_{0,\Omega}^2 \right)^{1/2} \left(\frac{1}{\lambda} \|\psi - \alpha q\|_{0,\Omega}^2 + c_0 \|q\|_{0,\Omega}^2 \right)^{1/2}, \end{aligned} \quad (2.25)$$

for all $\phi, \psi, p, q \in Q$, and

$$C((\psi, q), (\psi, q)) = \frac{1}{\lambda} \|\psi - \alpha q\|_{0,\Omega}^2 + c_0 \|q\|_{0,\Omega}^2 \geq c_0 \|q\|_{0,\Omega}^2. \quad (2.26)$$

Theorem 2.1. *Let $(\mathbf{u}, \phi, \boldsymbol{\sigma}, p) \in \mathbf{H} \times Q \times \mathbf{Z} \times Q$ be such that the system (2.17)–(2.20) holds. Then, there exists a constant $C > 0$, independent of λ , such that*

$$\|\mathbf{u}\|_{1,\Omega} + \|\phi\|_{0,\Omega} + \|\boldsymbol{\sigma}\|_{\text{div},\Omega} + \|p\|_{0,\Omega} \leq C(\|F_1\|_{\mathbf{H}'} + \|G_1\|_{Q'} + \|F_2\|_{\mathbf{Z}'} + \|G_2\|_{Q'}).$$

Proof. Proceeding similarly to the proof of Theorem 4.3.1 from [14], we will perform three steps. Firstly, we assume that $G_1 = 0$ and $F_2 = 0$ and bound the solution in terms of F_1 and G_2 . Secondly, we assume that $F_1 = 0$, $G_2 = 0$, $G_1 = 0$ and derive an estimate for the solution in terms of F_2 . Finally, we assume that $F_1 = 0$, $G_2 = 0$ and $F_2 = 0$ and derive an estimate for the solution in terms of G_1 . In this way, the desired stability will follow by linearity after adding the obtained estimates.

Step 1 ($G_1 = 0$ and $F_2 = 0$). Taking $\mathbf{v} = \mathbf{u}$ in (2.17), $\psi = \phi$ in (2.18), $\boldsymbol{\tau} = \boldsymbol{\sigma}$ in (2.8) and $q = p$ in (2.20) and performing the operations (2.17) – (2.18) + (2.19) – (2.20), we obtain

$$a_s(\mathbf{u}, \mathbf{u}) + a_f(\boldsymbol{\sigma}, \boldsymbol{\sigma}) + C((\phi, p), (\phi, p)) = F_1(\mathbf{u}) + G_2(p).$$

Then, applying (2.14), (2.26) and the boundedness of F_1 and G_2 in the identity above, we deduce that

$$2\mu C_{k,1} \|\mathbf{u}\|_{1,\Omega}^2 + c_0 \|p\|_{0,\Omega}^2 \leq \|F_1\|_{\mathbf{H}'} \|\mathbf{u}\|_{1,\Omega} + \|G_2\|_{Q'} \|p\|_{0,\Omega},$$

which implies that

$$\|\mathbf{u}\|_{1,\Omega} + \|p\|_{0,\Omega} \leq C_1(\|F_1\|_{\mathbf{H}'} + \|G_2\|_{Q'}), \quad (2.27)$$

with $C_1 > 0$ independent of λ . Then from the first condition in (2.16) and (2.18) we observe that

$$\beta_s \|\phi\|_{0,\Omega} \leq \sup_{\mathbf{v} \in \mathbf{H} \setminus \{\mathbf{0}\}} \frac{b_s(\mathbf{v}, \phi)}{\|\mathbf{v}\|_{1,\Omega}} = \sup_{\mathbf{v} \in \mathbf{H} \setminus \{\mathbf{0}\}} \frac{F_1(\mathbf{v}) - a_s(\mathbf{u}, \mathbf{v})}{\|\mathbf{v}\|_{1,\Omega}},$$

which together with (2.27) and the continuity of a_s and F_1 , implies

$$\|\phi\|_{0,\Omega} \leq C_2 (\|F_1\|_{\mathbf{H}'} + \|G_2\|_{Q'}), \quad (2.28)$$

with $C_2 > 0$ independent of λ .

Now, in order to bound $\|\boldsymbol{\sigma}\|_{\text{div},\Omega}$, we let $\boldsymbol{\sigma}_0 \in K_f$ and $\boldsymbol{\sigma}^\perp \in K_f^\perp$, such that $\boldsymbol{\sigma} = \boldsymbol{\sigma}_0 + \boldsymbol{\sigma}^\perp$. First, from (2.19) with $\boldsymbol{\tau} = \boldsymbol{\sigma}_0$ and noticing that $\boldsymbol{\sigma}_0 \in K_f$, we have

$$a_f(\boldsymbol{\sigma}_0, \boldsymbol{\sigma}_0) = -a_f(\boldsymbol{\sigma}^\perp, \boldsymbol{\sigma}_0),$$

which jointly with (2.15) and the continuity of a_f (cf. (2.11)), gives

$$\|\boldsymbol{\sigma}_0\|_{\text{div},\Omega} \leq \frac{\kappa_2}{\kappa_1} \|\boldsymbol{\sigma}^\perp\|_{\text{div},\Omega}. \quad (2.29)$$

In turn, combining the second condition in (2.16) with Lemma 2.1 of [29] and (2.20), we obtain

$$\beta_f \|\boldsymbol{\sigma}^\perp\|_{\text{div},\Omega} \leq \sup_{q \in Q \setminus \mathbf{0}} \frac{b_f(\boldsymbol{\sigma}, q)}{\|q\|_{0,\Omega}} = \sup_{q \in Q \setminus \mathbf{0}} \frac{G_2(q) - b_{sf}(\phi, q) - c_f(p, q)}{\|q\|_{0,\Omega}},$$

which together with the continuity of G_2 , b_{sf} and c_f (cf. (2.11)), estimates (2.27) and (2.28), yields

$$\|\boldsymbol{\sigma}^\perp\|_{\text{div},\Omega} \leq C \left(1 + \frac{2}{\lambda} + c_0 \right) (\|F_1\|_{\mathbf{H}'} + \|G_2\|_{Q'}), \quad (2.30)$$

where $1 + \frac{2}{\lambda} + c_0$ must be thought as a constant independent of λ if $\lambda \rightarrow \infty$. Then, from (2.29), (2.30) and the triangle inequality we easily deduce that

$$\|\boldsymbol{\sigma}\|_{\text{div},\Omega} \leq C_3 (\|F_1\|_{\mathbf{H}'} + \|G_2\|_{Q'}), \quad (2.31)$$

with $C_3 > 0$ independent of λ . We conclude the first step by observing that the aforementioned estimate follows from (2.27), (2.28) and (2.31).

Step 2 ($F_1 = 0$, $G_1 = 0$ and $G_2 = 0$). Now we proceed to bound the solution in terms of $\|F_2\|_{\mathbf{Z}'}$. To that end we recall the decomposition $F_2 = F_2^0 + F_2^\perp$ from (2.21). Consequently we bound the solution, firstly in terms of $\|F_2^\perp\|_{(K_f^\perp)'}^0$ (assuming that $F_2^0 = 0$), and secondly in terms of $\|F_2^0\|_{K_f'}$ (assuming that $F_2^\perp = 0$). Hence, the desired estimate follows by linearity, adding both estimates.

Let $\boldsymbol{\sigma}_0 \in K_f$ and $\boldsymbol{\sigma}^\perp \in K_f^\perp$ be such that $\boldsymbol{\sigma} = \boldsymbol{\sigma}_0 + \boldsymbol{\sigma}^\perp$. Similarly, we let $\mathbf{u}_0 \in K_s$ and $\mathbf{u}^\perp \in K_s^\perp$ be such that $\mathbf{u} = \mathbf{u}_0 + \mathbf{u}^\perp$. In turn, taking $\mathbf{v} = \mathbf{u}$ in (2.17), $\psi = \phi$ in (2.18), $\boldsymbol{\tau} = \boldsymbol{\sigma}$ in (2.19) and $q = p$ in (2.20) and performing the operations (2.17) – (2.18) + (2.19) – (2.20), we observe that there holds

$$a_s(\mathbf{u}, \mathbf{u}) + a_f(\boldsymbol{\sigma}, \boldsymbol{\sigma}) + C((\phi, p), (\phi, p)) = F_2^0(\boldsymbol{\sigma}_0) + F_2^\perp(\boldsymbol{\sigma}^\perp), \quad (2.32)$$

In addition, from (2.19) with $\boldsymbol{\tau} = \boldsymbol{\sigma}_0$ and (2.22) we notice that

$$a_f(\boldsymbol{\sigma}_0, \boldsymbol{\sigma}_0) + a_f(\boldsymbol{\sigma}^\perp, \boldsymbol{\sigma}_0) = F_2^0(\boldsymbol{\sigma}_0). \quad (2.33)$$

$F_2^0 = 0$. We begin by noticing that from (2.32) there holds

$$C((\phi, p), (\phi, p)) \leq F_2^\perp(\boldsymbol{\sigma}^\perp), \quad (2.34)$$

and since $F_2^0 = 0$, from (2.33), and from the continuity and ellipticity of a_f , we have

$$\|\boldsymbol{\sigma}_0\|_{\text{div},\Omega} \leq \frac{\kappa_2}{\kappa_1} \|\boldsymbol{\sigma}^\perp\|_{\text{div},\Omega}. \quad (2.35)$$

Moreover, summing up equations (2.18) and (2.20), we deduce that

$$b_s(\mathbf{u}^\perp, \psi) + b_f(\boldsymbol{\sigma}^\perp, q) = C((\phi, p), (\psi, q)) \quad \forall \psi, q \in Q,$$

which together with (2.24), (2.25) and (2.34) implies

$$\begin{aligned} \beta \|\boldsymbol{\sigma}^\perp\|_{\text{div},\Omega} &\leq \sup_{(\psi, q) \in (Q \times Q) \setminus \mathbf{0}} \frac{b_s(\mathbf{u}^\perp, \psi) + b_f(\boldsymbol{\sigma}^\perp, q)}{\|\psi\|_{0,\Omega} + \|q\|_{0,\Omega}} = \sup_{(\psi, q) \in (Q \times Q) \setminus \mathbf{0}} \frac{C((\phi, p), (\psi, q))}{\|\psi\|_{0,\Omega} + \|q\|_{0,\Omega}} \\ &\leq \left(\frac{1}{\lambda} \|\phi - \alpha p\|_{0,\Omega}^2 + c_0 \|p\|_{0,\Omega}^2 \right)^{1/2} \sup_{(\psi, q) \in (Q \times Q) \setminus \mathbf{0}} \frac{\left(\frac{1}{\lambda} \|\psi - \alpha q\|_{0,\Omega}^2 + c_0 \|q\|_{0,\Omega}^2 \right)^{1/2}}{\|\psi\|_{0,\Omega} + \|q\|_{0,\Omega}} \\ &\leq (F_2^\perp(\boldsymbol{\sigma}^\perp))^{1/2} \sup_{(\psi, q) \in (Q \times Q) \setminus \mathbf{0}} \frac{\left(\frac{1}{\lambda} \|\psi - \alpha q\|_{0,\Omega}^2 + c_0 \|q\|_{0,\Omega}^2 \right)^{1/2}}{\|\psi\|_{0,\Omega} + \|q\|_{0,\Omega}}. \end{aligned} \quad (2.36)$$

Then, defining

$$C_c = \sup_{(\psi, q) \in (Q \times Q) \setminus \mathbf{0}} \frac{\left(\frac{1}{\lambda} \|\psi - \alpha q\|_{0,\Omega}^2 + c_0 \|q\|_{0,\Omega}^2 \right)^{1/2}}{\|\psi\|_{0,\Omega} + \|q\|_{0,\Omega}}, \quad (2.37)$$

which can be seen as a constant independent of λ if $\lambda \rightarrow \infty$, from (2.36) we obtain

$$\|\boldsymbol{\sigma}^\perp\|_{\text{div},\Omega} \leq \frac{C_c^2}{\beta^2} \|F_2^\perp\|_{(K_f^\perp)'} \quad (2.38)$$

Hence, combining (2.32) and (2.38) together with (2.14) and (2.26), we can easily deduce that

$$\|\mathbf{u}\|_{1,\Omega} + \|p\|_{0,\Omega} \leq C_4 \|F_2^\perp\|_{(K_f^\perp)'}, \quad (2.39)$$

with $C_4 > 0$ independent of λ . Moreover, from (2.35), (2.38) and the triangle inequality we also get

$$\|\boldsymbol{\sigma}\|_{\text{div},\Omega} \leq \|\boldsymbol{\sigma}_0\|_{\text{div},\Omega} + \|\boldsymbol{\sigma}^\perp\|_{\text{div},\Omega} \leq \left(1 + \frac{\kappa_2}{\kappa_1} \right) \|\boldsymbol{\sigma}^\perp\|_{\text{div},\Omega} \leq C_5 \|F_2^\perp\|_{(K_f^\perp)'}, \quad (2.40)$$

with $C_5 > 0$ independent of λ . Finally, using the inf-sup condition (2.16) and proceeding similarly as for the derivation of (2.28), we can obtain

$$\|\phi\|_{0,\Omega} \leq C_6 \|F_2^\perp\|_{(K_f^\perp)'} \quad (2.41)$$

with $C_6 > 0$ independent of λ . In this way from (2.39) to (2.41) we obtain the result for the case $F_2^0 = 0$. $F_2^\perp = 0$. First, from (2.32) and (2.33) we obtain, respectively

$$\frac{1}{\lambda} \|\phi - \alpha p\|_{0,\Omega}^2 + c_0 \|p\|_{0,\Omega}^2 \leq F_2^0(\boldsymbol{\sigma}_0), \quad (2.42)$$

and

$$\|\boldsymbol{\sigma}_0\|_{\text{div},\Omega} \leq \frac{\kappa_2}{\kappa_1} \|\boldsymbol{\sigma}^\perp\|_{\text{div},\Omega} + \frac{2\kappa_2}{\eta} \|F_2^0\|_{K_f'}. \quad (2.43)$$

Now, similarly as in (2.36), from the inf-sup condition (2.24), estimates (2.25) and (2.42), and recalling the definition of the constant C_c in (2.37), we obtain

$$\beta \|\boldsymbol{\sigma}^\perp\|_{\text{div},\Omega} \leq C_c (F_2^0(\boldsymbol{\sigma}_0))^{1/2} \leq C_c \|F_2^0\|_{K_f'}^{1/2} \|\boldsymbol{\sigma}_0\|_{\text{div},\Omega}^{1/2},$$

which, associated with (2.43) and Young's inequality, yields

$$\|\boldsymbol{\sigma}^\perp\|_{\text{div},\Omega} \leq C\|F_2^0\|_{K_f'} + \tilde{C}\|F_2^0\|_{K_f'}^{1/2}\|\boldsymbol{\sigma}^\perp\|_{\text{div},\Omega}^{1/2} \leq \hat{C}\|F_2^0\|_{K_f'} + \frac{1}{2}\|\boldsymbol{\sigma}^\perp\|_{\text{div},\Omega},$$

and therefore

$$\|\boldsymbol{\sigma}^\perp\|_{\text{div},\Omega} \leq 2\hat{C}\|F_2^0\|_{K_f'}, \quad (2.44)$$

with \hat{C} independent of λ . Notice that from the latter and estimate (2.43) it readily follows that

$$\|\boldsymbol{\sigma}_0\|_{\text{div},\Omega} \leq \bar{C}\|F_2^0\|_{K_f'}. \quad (2.45)$$

In this way, from (2.44), (2.45) and the triangle inequality, we can assert that

$$\|\boldsymbol{\sigma}\|_{\text{div},\Omega} \leq C_7\|F_2^0\|_{K_f'}, \quad (2.46)$$

with $C_7 > 0$ independent of λ . Moreover, from (2.14), (2.32) and (2.45) we can deduce that

$$\|\mathbf{u}\|_{1,\Omega} + \|p\|_{0,\Omega} \leq C_8\|F_2^0\|_{K_f'}, \quad (2.47)$$

with $C_8 > 0$ independent of λ , and to conclude, analogously to (2.28), from the inf-sup condition (2.16), equation (2.18) and (2.47), we obtain

$$\|\phi\|_{0,\Omega} \leq C_9\|F_2^0\|_{K_f'}, \quad (2.48)$$

with $C_9 > 0$ independent of λ . The desired estimate then follows from (2.46) to (2.48).

Step 3 ($F_1 = 0$, $G_2 = 0$ and $F_2 = 0$). Once again we let $\boldsymbol{\sigma}_0 \in K_f$ and $\boldsymbol{\sigma}^\perp \in K_f^\perp$ be such that $\boldsymbol{\sigma} = \boldsymbol{\sigma}_0 + \boldsymbol{\sigma}^\perp$ and $\mathbf{u}_0 \in K_s$ and $\mathbf{u}^\perp \in K_s^\perp$ satisfying $\mathbf{u} = \mathbf{u}_0 + \mathbf{u}^\perp$, and observe that there holds

$$a_s(\mathbf{u}, \mathbf{u}) + a_f(\boldsymbol{\sigma}, \boldsymbol{\sigma}) + C((\phi, p), (\phi, p)) = G_1(\phi), \quad (2.49)$$

and

$$b_s(\mathbf{u}^\perp, \psi) + b_f(\boldsymbol{\sigma}^\perp, q) - C((\phi, p), (\psi, q)) = G_1(\psi) \quad \forall \psi, q \in Q.$$

In particular, from the latter and the inf-sup condition (2.24) we obtain

$$\begin{aligned} \beta(\|\mathbf{u}^\perp\|_{1,\Omega} + \|\boldsymbol{\sigma}^\perp\|_{\text{div},\Omega}) &\leq \sup_{(\psi, q) \in (Q \times Q) \setminus \mathbf{0}} \frac{b_s(\mathbf{u}^\perp, \psi) + b_f(\boldsymbol{\sigma}^\perp, q)}{\|\psi\|_{0,\Omega} + \|q\|_{0,\Omega}} \\ &= \sup_{(\psi, q) \in (Q \times Q) \setminus \mathbf{0}} \frac{G_1(\psi) + C((\phi, p), (\psi, q))}{\|\psi\|_{0,\Omega} + \|q\|_{0,\Omega}}, \end{aligned}$$

which together with (2.25), (2.49) and the continuity of G_1 , gives the bound

$$\begin{aligned} \beta(\|\mathbf{u}^\perp\|_{1,\Omega} + \|\boldsymbol{\sigma}^\perp\|_{\text{div},\Omega}) &\leq \|G_1\|_{Q'} + C_c\{C((\phi, p), (\phi, p))\}^{1/2} \\ &\leq \|G_1\|_{Q'} + C_c\|G_1\|_{Q'}^{1/2}\|\phi\|_{0,\Omega}^{1/2}. \end{aligned} \quad (2.50)$$

where $C_c > 0$ is the constant defined in (2.37). Now, from (2.17) with $\mathbf{v} = \mathbf{u}_0$ and using the ellipticity and continuity of a_s (cf. (2.14) and (2.11), respectively), it readily follows that

$$\|\mathbf{u}_0\|_{1,\Omega} \leq \frac{C_{k,2}}{C_{k,1}}\|\mathbf{u}^\perp\|_{1,\Omega},$$

which implies

$$\|\mathbf{u}\|_{1,\Omega} \leq \left(1 + \frac{C_{k,2}}{C_{k,1}}\right)\|\mathbf{u}^\perp\|_{1,\Omega}. \quad (2.51)$$

The latter, the inf-sup condition (2.16) and equation (2.17) yield

$$\|\phi\|_{0,\Omega} \leq \beta_s^{-1} \sup_{\mathbf{v} \in \mathbf{H} \setminus \mathbf{0}} \frac{b_s(\mathbf{v}, \phi)}{\|\mathbf{v}\|_{1,\Omega}} \leq \beta_s^{-1} \sup_{\mathbf{v} \in \mathbf{H} \setminus \mathbf{0}} \frac{-a_s(\mathbf{u}, \mathbf{v})}{\|\mathbf{v}\|_{1,\Omega}} \leq 2\mu\beta_s^{-1}C_{k,2}\|\mathbf{u}\|_{1,\Omega} \leq \hat{C}_1\|\mathbf{u}^\perp\|_{1,\Omega}, \quad (2.52)$$

with $\hat{C}_1 > 0$ independent of λ . Then, combining (2.50) and (2.52) with Young's inequality, we obtain

$$\|\mathbf{u}^\perp\|_{1,\Omega} \leq \hat{C}_2\|G_1\|_{Q'}$$

Using this inequality, from (2.51) and (2.52), we easily get

$$\|\mathbf{u}\|_{1,\Omega} \leq \hat{C}_3\|G_1\|_{Q'} \quad \text{and} \quad \|\phi\|_{0,\Omega} \leq \hat{C}_4\|G_1\|_{Q'}, \quad (2.53)$$

with $\hat{C}_3 > 0$ and $\hat{C}_4 > 0$ independent of λ . In turn, similarly as in (2.29) we can assert that

$$\|\boldsymbol{\sigma}_0\|_{\text{div},\Omega} \leq \frac{\kappa_2}{\kappa_1}\|\boldsymbol{\sigma}^\perp\|_{\text{div},\Omega},$$

and invoking (2.50) and (2.53) we can derive the bound

$$\|\boldsymbol{\sigma}\|_{\text{div},\Omega} \leq \hat{C}_5\|G_1\|_{Q'}, \quad (2.54)$$

with $\hat{C}_5 > 0$ independent of λ . Finally, from the second inf-sup condition in (2.16), equation (2.19) and estimate (2.54) there holds

$$\|p\|_{0,\Omega} \leq \hat{C}_6\|G_1\|_{Q'}. \quad (2.55)$$

In this way, from (2.53) to (2.55) we obtain the desired estimate, which concludes the proof. \square

As a consequence of Theorem 2.1 we can readily deduce the following result.

Theorem 2.2. *There exists a unique $(\mathbf{u}, \phi, \boldsymbol{\sigma}, p) \in \mathbf{H} \times Q \times \mathbf{Z} \times Q$ satisfying (2.6)–(2.9). Moreover, there exists $C > 0$, independent of λ , such that*

$$\|\mathbf{u}\|_{1,\Omega} + \|\phi\|_{0,\Omega} + \|\boldsymbol{\sigma}\|_{\text{div},\Omega} + \|p\|_{0,\Omega} \leq C_{\text{stab}}(\|\mathbf{f}\|_{0,\Omega} + \|\mathbf{g}\|_{0,\Omega} + \|\ell\|_{0,\Omega} + \|p_\Gamma\|_{1/2,00,\Gamma_p}).$$

Proof. By setting $F_1, F_2 = 0$ and $G_1, G_2 = 0$ in (2.17)–(2.20) from Theorem 2.1 we can readily deduce the uniqueness of solution of problem (2.6)–(2.9). Furthermore, noticing that (2.6)–(2.9) is a symmetric linear problem, the above also guarantees existence of solution, which completes the solvability analysis. In turn, by setting $F_1 = F$, $G_1 = 0$, $F_2 = G$ and $G_2 = H$, the continuous dependence result is a direct consequence of Theorem 2.1 and (2.12), which concludes the proof. \square

Notice that in the proof of the preceding theorem, to obtain the estimate for p we use explicitly that $c_f(p, p) = c_0\|p\|_{0,\Omega}^2$, and consequently C_{stab} is a constant depending on $1/c_0$ (see for instance estimate (2.27)). Therefore, for the limit case $c_0 = 0$ (*i.e.* a medium with incompressible solid grains) the analysis above is not straightforwardly applicable. If $c_0 = 0$ one can still proceed similarly to the proof of Theorem 4.3.1 from [14] to obtain the stability result but unfortunately with a constant depending on λ . However, numerical evidence shows that our method is still stable even if $c_0 = 0$ or small enough (see Examples 2 and 3 in Sect. 6, below), which suggests that for the case $c_0 = 0$ the analysis might be derived using a different approach.

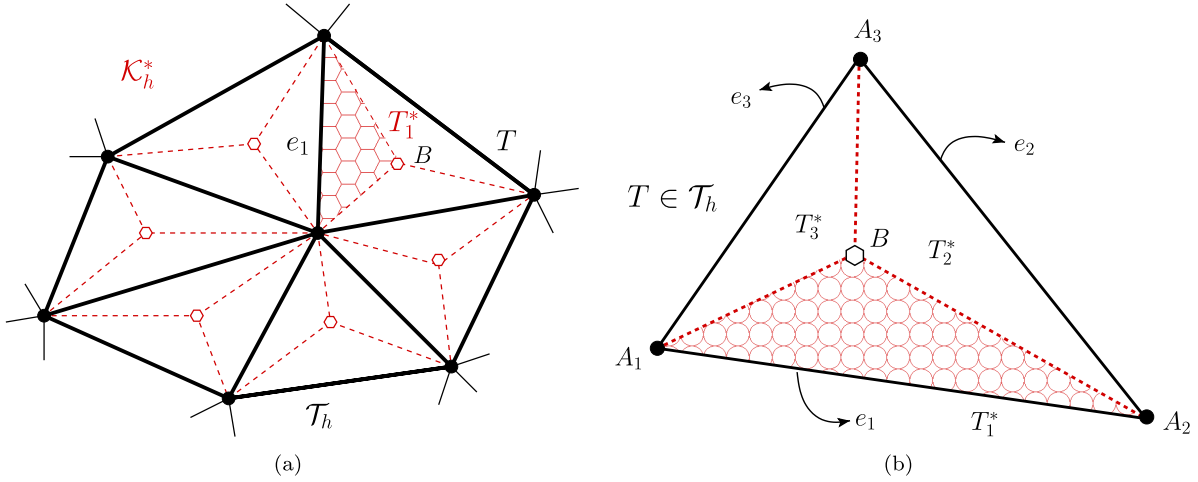


FIGURE 1. A compound of six elements in \mathcal{T}_h (a), and barycentric subdivision of a given $T \in \mathcal{T}_h$ into three control volumes T_j^* belonging to the dual mesh \mathcal{K}_h^* (b). The vertices of \mathcal{T}_h are labelled with A_i , and the edges of primal elements are denoted e_i .

3. DISCONTINUOUS FINITE VOLUMES – MIXED FINITE ELEMENTS

3.1. Primal and dual meshes

The construction of DFV-MFE schemes can be straightforwardly carried out for $d = 2, 3$; however, for sake of conciseness, we will restrict the presentation to the 2D case. We stress that by following the analysis of [37] and [17], the present analysis can be easily extended to 3D case. Let us then consider a family $\{\mathcal{T}_h\}_{h>0}$ of regular, quasi-uniform partitions of $\bar{\Omega}$ into triangles T of diameter h_T , where $h = \max\{h_T : T \in \mathcal{T}_h\}$ is the meshsize. We will refer to these triangulations as *primal meshes*.

Let \mathcal{E}_h denote the set of interior edges in the primal mesh and write $\mathcal{E}_h(T)$ for its localisation to the element $T \in \mathcal{T}_h$. Moreover, let $e \in \mathcal{E}_h$ be shared by two elements T_1 and T_2 in \mathcal{T}_h with outward unit normal vectors \mathbf{n}_1 and \mathbf{n}_2 , respectively. For a scalar q , we will write $\llbracket q \rrbracket := q|_{\partial T_1} - q|_{\partial T_2}$ and $\{\{q\}\} := \frac{1}{2}(q|_{\partial T_1} + q|_{\partial T_2})$ to denote its jump and average values on e , respectively. For a generic vector \mathbf{r} , its vector jump and vectorial average across edge e is denoted respectively, by $\llbracket \mathbf{r} \rrbracket := \mathbf{r}|_{\partial T_1} - \mathbf{r}|_{\partial T_2}$ and $\{\{\mathbf{r}\}\} := \frac{1}{2}(\mathbf{r}|_{\partial T_1} + \mathbf{r}|_{\partial T_2})$.

In order to define DFV approximations for the solid displacements, we construct an auxiliary, *dual mesh*. Starting from a given triangle T in the primal mesh \mathcal{T}_h , we proceed to divide it into three sub-triangles by joining the barycentre B to the vertices of T . The dual mesh, denoted by \mathcal{K}_h^* , will then consist of all these *control volumes*, T^* , generated after barycentric subdivision. A sketch of the subdivision in a given T and also a compound of six primal elements is presented in Figure 1.

3.2. Discrete trial and test spaces

Specifying the trial and test spaces will completely characterise the DFV method. Let us introduce the trial space for the approximation of solid displacements as

$$\mathbf{H}_h := \{\mathbf{v}_h \in \mathbf{L}^2(\Omega) : \mathbf{v}_h|_T \in \mathcal{P}_1(T)^2 \quad \forall T \in \mathcal{T}_h\},$$

whereas the corresponding test space will be associated with the dual mesh \mathcal{K}_h^* , and will be defined as

$$\mathbf{H}_h^* := \{\mathbf{v}_h \in \mathbf{L}^2(\Omega) : \mathbf{v}_h|_T^* \in \mathcal{P}_0(T^*)^2 \quad \forall T^* \in \mathcal{K}_h^*\}.$$

Here $\mathcal{P}_k(T)$ denotes the space of polynomials of degree less than or equal than k defined over the element T . One readily notices that given the specific form of control volumes, the linear systems arising from the discretisation of operators involving the solid displacement approximation will be square. Moreover, we observe that the dual elements have support only in the primal triangle they belong to (in contrast to conforming FVE schemes, where the control volumes have a support shared on the neighbouring triangles in the primal mesh, see *e.g.* [5]). Such localisation property may turn the method more amenable for parallelisation and eventual implementation of adaptive DFV schemes.

Next, let us define $\mathbf{H}(h) := \mathbf{H}_h + [\mathbf{H}^2(\Omega) \cap \mathbf{H}_{\Gamma_u}^1(\Omega)]$, and introduce a mapping that connects this modified trial space with the test space as follows

$$R_h : \mathbf{H}(h) \longrightarrow \mathbf{H}_h^*, \quad \mathbf{v}|_{T^*} \mapsto R_h \mathbf{v}|_{T^*} := \frac{1}{h_e} \int_e \mathbf{v}|_{T^*}, \quad T^* \in \mathcal{K}_h^*,$$

where h_e denotes the length of the generic edge e of the primal element T that contains the control volume T^* (see Fig. 1b). We provide $\mathbf{H}(h)$ with the mesh-dependent norm $\|\cdot\|_h$, defined as

$$\|\mathbf{v}\|_h^2 := |\mathbf{v}|_{1,h}^2 + \sum_{e \in \mathcal{E}_h} \frac{1}{h_e} \int_e [\mathbf{v}]^2,$$

which uses the broken \mathbf{H} -semi-norm $|\mathbf{v}|_{1,h}^2 = \sum_{T \in \mathcal{T}_h} |\mathbf{v}|_{1,T}^2$.

On the other hand, we consider the finite dimensional space associated with the approximation of the fluid flux and the fluid pressure as the mixed finite element constituted by the lowest order Raviart–Thomas space and the space of piecewise constants defined over the primal mesh

$$\begin{aligned} \mathbf{Z}_h &:= \{\boldsymbol{\tau}_h \in \mathbf{Z} : \boldsymbol{\tau}_h|_T \in \mathcal{RT}_0(T), \forall T \in \mathcal{T}_h, \text{ and } \boldsymbol{\tau}_h \cdot \mathbf{n} = 0 \text{ on } \Gamma_u\}, \\ Q_h &:= \{q_h \in Q : q_h|_T \text{ is a constant, } \forall T \in \mathcal{T}_h\}, \end{aligned}$$

where \mathcal{RT}_0 denotes the local Raviart–Thomas space of lowest order. The trial and test spaces for the approximation of the total pressure will coincide with the ones used for the fluid pressure.

Boundary or transmission conditions could be alternatively set up using appropriate Lagrange multipliers (see *e.g.* the recent analysis in [3]), in which case appropriate compatibility conditions should be required between the interior and boundary meshes.

3.3. The conservative discrete formulation

Applying then a combined DFV-MFE discretisation, we end up with the following formulation: Find $(\mathbf{u}_h, \phi_h, \boldsymbol{\sigma}_h, p_h) \in \mathbf{H}_h \times Q_h \times \mathbf{Z}_h \times Q_h$ such that

$$a_s^h(\mathbf{u}_h, \mathbf{v}_h) + b_s^h(\mathbf{v}_h, \phi_h) = F(R_h \mathbf{v}_h) \quad \forall \mathbf{v}_h \in \mathbf{H}_h, \quad (3.1)$$

$$\tilde{b}_s^h(\mathbf{u}_h, \psi_h) - c_s(\phi_h, \psi_h) + b_{sf}(\psi_h, p_h) = 0 \quad \forall \psi_h \in Q_h, \quad (3.2)$$

$$a_f(\boldsymbol{\sigma}_h, \boldsymbol{\tau}_h) + b_f(\boldsymbol{\tau}_h, p_h) = G(\boldsymbol{\tau}_h) \quad \forall \boldsymbol{\tau}_h \in \mathbf{Z}_h, \quad (3.3)$$

$$b_{sf}(\phi_h, q_h) + b_f(\boldsymbol{\sigma}_h, q_h) - c_f(p_h, q_h) = H(q_h) \quad \forall q_h \in Q_h, \quad (3.4)$$

where the three bilinear forms that are modified with respect to the ones specified in (2.10), are now defined as follows

$$\begin{aligned} a_s^h(\mathbf{u}_h, \mathbf{v}_h) &:= -2\mu \sum_{T \in \mathcal{T}_h} \sum_{j=1}^3 \int_{A_{j+1} \cup A_j} \boldsymbol{\varepsilon}(\mathbf{u}_h) \mathbf{n} \cdot R_h \mathbf{v}_h - 2\mu \sum_{e \in \mathcal{E}_h} \langle [\![R_h \mathbf{v}_h]\!], \{ \boldsymbol{\varepsilon}(\mathbf{u}_h) \mathbf{n} \} \rangle_e \\ &\quad - 2\theta\mu \sum_{e \in \mathcal{E}_h \cup \Gamma_u} \langle [\![R_h \mathbf{u}_h]\!], \{ \boldsymbol{\varepsilon}(\mathbf{v}_h) \mathbf{n} \} \rangle_e + \sum_{e \in \mathcal{E}_h \cup \Gamma_u} 2\mu \frac{\gamma_u}{h_e} \langle [\![\mathbf{u}_h]\!], [\![\mathbf{v}_h]\!] \rangle_e, \end{aligned}$$

$$b_s^h(\mathbf{v}_h, \psi_h) := \sum_{T \in \mathcal{T}_h} \sum_{j=1}^3 \int_{A_{j+1} \cap BA_j} \psi_h R_h \mathbf{v}_h \cdot \mathbf{n} + \sum_{e \in \mathcal{E}_h} \langle \{\!\{ \psi_h \mathbf{n} \}\!\}, \llbracket R_h \mathbf{v}_h \rrbracket \rangle_e,$$

$$\tilde{b}_s^h(\mathbf{u}_h, \psi_h) := - \int_{\Omega} \psi_h \operatorname{div} \mathbf{u}_h + \sum_{e \in \mathcal{E}_h \cup \Gamma_{\mathbf{u}}} \langle \{\!\{ \psi_h \mathbf{n} \}\!\}, \llbracket R_h \mathbf{u}_h \rrbracket \rangle_e,$$

with $A_4 = A_1$ (see Fig. 1b), and where $\gamma_{\mathbf{u}} > 0$ is a penalty parameter independent of h (see *e.g.* the DFV formulations for Stokes equations proposed in [37, 64]). The symmetrisation parameter $\theta \in \{1, 0, -1\}$ leads respectively to symmetric, incomplete, and non-symmetric interior penalty DG formulations. We recall that for boundary edges we adopt the convention that $\{\!\{ \mathbf{r} \}\!\} = \mathbf{r}$ and $\llbracket \mathbf{r} \rrbracket = \mathbf{r}$, for a generic vector field \mathbf{r} . We also note that the edge integrals on $\Gamma_{\mathbf{u}}$ are required only if the Dirichlet boundary conditions for displacements are implemented using Nitsche's approach.

4. SOLVABILITY AND STABILITY OF THE DISCRETE PROBLEM

4.1. Preliminaries

The unique solvability of the discrete problem (3.1)–(3.4) can be established by proving that the sole feasible solution to the homogeneous counterpart of the system is the trivial one. We start by collecting some useful results to be exploited in the sequel.

First, for any $\mathbf{v} \in \mathbf{H}^1(T)$ and for any edge $e \in \mathcal{E}_h(T)$ one has the trace inequality (*cf.* [6])

$$\|\mathbf{v}\|_{0,e}^2 \leq C \left(h_e^{-1} \|\mathbf{v}\|_{0,T}^2 + h_e |\mathbf{v}|_{1,T}^2 \right). \quad (4.1)$$

Secondly, the bilinear forms $a_s^h(\cdot, \cdot)$, $\tilde{b}_s^h(\cdot, \cdot)$ and $b_1^h(\cdot, \cdot)$ hold the following set of properties (continuity, positivity, and suitable inf-sup conditions). There exist constants $C_i > 0, \beta_0 > 0$ independent of the meshsize h , such that

$$a_s^h(\mathbf{v}_h, \mathbf{w}_h) \leq C_1 \|\mathbf{v}_h\|_h \|\mathbf{w}_h\|_h \quad \forall \mathbf{v}_h, \mathbf{w}_h \in \mathbf{H}(h), \quad (4.2)$$

$$a_s^h(\mathbf{v}_h, \mathbf{v}_h) \geq C_2 \|\mathbf{v}_h\|_h^2 \quad \forall \mathbf{v}_h \in \mathbf{H}_h, \quad (4.3)$$

$$b_s^h(\mathbf{v}_h, \psi_h) \leq C_3 \|\mathbf{v}_h\|_h \|\psi_h\|_{0,\Omega} \quad \forall \mathbf{v}_h \in \mathbf{H}(h), \psi_h \in \mathbf{Q}_h, \quad (4.4)$$

$$\sup_{\mathbf{v}_h \neq \mathbf{0} \in \mathbf{H}_h} \frac{\tilde{b}_s^h(\mathbf{v}_h, \psi_h)}{\|\mathbf{v}_h\|_h} \geq \beta_0 \|\psi_h\|_{0,\Omega} \quad \forall \psi_h \in \mathbf{Q}_h, \quad (4.5)$$

$$b_s^h(\mathbf{v}_h, \psi_h) = \tilde{b}_s^h(\mathbf{v}_h, \psi_h) \quad \forall \mathbf{v}_h \in \mathbf{H}(h), \psi_h \in \mathbf{Q}_h. \quad (4.6)$$

For a proof of (4.2) and (4.3) we refer to Lemma 4 of [37], whereas the bounds (4.4), (4.5), as well as the equivalence (4.6) can be found respectively in Lemmas 3.4, 4.1 and 3.2 from [64]. In particular, from (4.4) and the inverse inequality $|\psi_h|_{1,T} \leq Ch^{-1} \|\psi_h\|_{0,T}$, for all $\phi_h \in \mathbf{Q}_h$ and for all $T \in \mathcal{T}_h$, with $C > 0$ independent of h (see for instance [25], Lem. 1.44), it follows that

$$b_s^h(\mathbf{v}_h, \psi_h) \leq \tilde{C}_3 \|\mathbf{v}_h\|_h \|\psi_h\|_{0,\Omega} \quad \forall \mathbf{v}_h \in \mathbf{H}(h), \psi_h \in \mathbf{Q}_h. \quad (4.7)$$

Let us now establish the stability properties of the forms a_f , b_f and c_f . We begin by recalling that, since $\operatorname{div} \mathbf{Z}_h \subseteq \mathbf{Q}_h$, the kernel of the bilinear form b_f can be characterised as follows

$$\mathbf{K}_h := \{ \boldsymbol{\tau}_h \in \mathbf{Z}_h : b_f(\boldsymbol{\tau}_h, q_h) = 0 \quad \forall q_h \in \mathbf{Q}_h \} = \{ \boldsymbol{\tau}_h \in \mathbf{Z}_h : \operatorname{div} \boldsymbol{\tau}_h = 0 \quad \text{in } \Omega \}.$$

Then, the \mathbf{K}_h -ellipticity of the bilinear form a_f is straightforward

$$a_f(\boldsymbol{\tau}_h, \boldsymbol{\tau}_h) \geq \frac{\eta}{\kappa} \|\boldsymbol{\tau}_h\|_{\operatorname{div}, \Omega}^2 \quad \forall \boldsymbol{\tau}_h \in \mathbf{K}_h.$$

In turn, it is well-known that the bilinear form b_f satisfies the following inf-sup condition

$$\sup_{\boldsymbol{\tau}_h \in \mathbf{Z}_h \setminus \{\mathbf{0}\}} \frac{b_f(\boldsymbol{\tau}_h, q_h)}{\|\boldsymbol{\tau}_h\|_{\text{div}, \Omega}} \geq \widehat{\beta} \|q_h\|_{0, \Omega} \quad \forall q_h \in Q_h,$$

with $\widehat{\beta} > 0$ independent of h (see [29], Sect. 4.2).

We point out that the continuity of the forms c_s , b_{sf} , a_f , b_f , c_f , as well as the functionals G and H are inherited from the continuous case, preserving the exact same continuity constants.

4.2. Well-posedness of the discrete scheme

We proceed similarly to the continuous case, and establish continuous dependence on data for (3.1)–(3.4) considering generic functionals, that is, we let $F_1^h \in \mathbf{H}'_h$, $G_1^h \in Q'_h$, $F_2^h \in \mathbf{Z}'_h$ and $G_2^h \in Q'_h$ and bound $\mathbf{u}_h \in \mathbf{H}_h$, $\phi_h \in Q_h$, $\boldsymbol{\sigma}_h \in \mathbf{Z}_h$ and $p_h \in Q_h$, satisfying

$$a_s^h(\mathbf{u}_h, \mathbf{v}_h) + b_s^h(\mathbf{v}_h, \phi_h) = F_1^h(\mathbf{v}_h) \quad \forall \mathbf{v}_h \in \mathbf{H}_h, \quad (4.8)$$

$$\tilde{b}_s^h(\mathbf{u}_h, \psi_h) - c_s(\phi_h, \psi_h) + b_{sf}(\psi_h, p_h) = G_1^h(\psi_h) \quad \forall \psi_h \in Q_h, \quad (4.9)$$

$$a_f(\boldsymbol{\sigma}_h, \boldsymbol{\tau}_h) + b_f(\boldsymbol{\tau}_h, p_h) = F_2^h(\boldsymbol{\tau}_h) \quad \forall \boldsymbol{\tau}_h \in \mathbf{Z}_h, \quad (4.10)$$

$$b_{sf}(\phi_h, q_h) + b_f(\boldsymbol{\sigma}_h, q_h) - c_f(p_h, q_h) = G_2^h(q_h) \quad \forall q_h \in Q_h, \quad (4.11)$$

in terms of the aforementioned functionals F_1^h , G_1^h , F_2^h and G_2^h . This result is established next.

Theorem 4.1. *Let $(\mathbf{u}_h, \phi_h, \boldsymbol{\sigma}_h, p_h) \in \mathbf{H}_h \times Q_h \times \mathbf{Z}_h \times Q_h$ satisfy the system of equations (4.8)–(4.11). Then, there exists a constant $\widehat{C} > 0$, independent of h and λ , such that*

$$\|\mathbf{u}_h\|_h + \|\phi_h\|_{0, \Omega} + \|\boldsymbol{\sigma}_h\|_{\text{div}, \Omega} + \|p_h\|_{0, \Omega} \leq \widehat{C}(\|F_1^h\|_{\mathbf{H}'_h} + \|G_1^h\|_{Q'_h} + \|F_2^h\|_{\mathbf{Z}'_h} + \|G_2^h\|_{Q'_h}). \quad (4.12)$$

Proof. Employing the discrete version of the stability properties of the forms involved, and proceeding analogously to the proof of Theorem 2.1, we can straightforwardly derive (4.12). \square

Now we are in position of establishing the well-posedness and stability of (3.1)–(3.4).

Theorem 4.2. *There exists a unique $(\mathbf{u}_h, \phi_h, \boldsymbol{\sigma}_h, p_h) \in \mathbf{H}_h \times Q_h \times \mathbf{Z}_h \times Q_h$ solution of the system (3.1)–(3.4). Moreover, there exists a constant $\widehat{C}_{\text{stab}} > 0$, independent of λ , such that*

$$\|\mathbf{u}_h\|_h + \|\phi_h\|_{0, \Omega} + \|\boldsymbol{\sigma}_h\|_{\text{div}, \Omega} + \|p_h\|_{0, \Omega} \leq \widehat{C}_{\text{stab}}(\|\mathbf{f}\|_{0, \Gamma} + \|\mathbf{g}\|_{0, \Omega} + \|\ell\|_{0, \Omega} + \|p_\Gamma\|_{1/2, 00, \Gamma_p}). \quad (4.13)$$

Proof. By setting $F_1^h = 0$, $G_1^h = 0$, $F_2^h = 0$ and $G_2^h = 0$ in (4.8)–(4.11) from Theorem 4.1 it follows that $\mathbf{u}_h = \mathbf{0}$, $\phi_h = 0$, $\boldsymbol{\sigma}_h = \mathbf{0}$ and $p_h = 0$ which implies that the only solution of the homogeneous problem is the trivial solution. From the latter, and from the fact that for finite dimensional linear problems existence and uniqueness of solution are equivalent, we readily obtain the well-posedness of (3.1)–(3.4). Moreover, by setting $F_1^h = FR_h|_{\mathbf{H}_h}$, $G_1^h = 0$, $F_2^h = G|_{\mathbf{Z}_h}$ and $G_2^h = H|_{Q_h}$ in (4.8)–(4.11) from (4.12) we easily obtain (4.13), which concludes the proof. \square

5. ERROR ESTIMATE

5.1. Preliminaries

Given $k \geq 0$, on each primal element $T \in \mathcal{T}_h$, let $\Lambda_k^T : L^2(T) \rightarrow \mathcal{P}_k(T)$ denote the orthogonal L^2 -projection operator, which satisfies the following approximation property (see, for instance, [38]): For all $s \in \{0, \dots, k+1\}$, there holds

$$|v - \Lambda_k^T v|_{m, T} \leq Ch_T^{s-m} |v|_{s, T} \quad \forall v \in H^m(T), \forall m \in \{0, \dots, s\}. \quad (5.1)$$

We will also use a vector version of Λ_k^T , say $\mathbf{\Lambda}_k^T : \mathbf{L}^2(T) \rightarrow \mathbf{P}_k(T)$, which is defined component-wise by Λ_k^T . Then, we define the global operators $\mathbf{\Pi}_1 : \mathbf{H}(h) \rightarrow \mathbf{H}_h$ and $\Lambda_0 : \mathbf{Q} \rightarrow \mathbf{Q}_h$ by

$$(\mathbf{\Pi}_1 \mathbf{v})|_T := \mathbf{\Lambda}_1^T \mathbf{v}, \quad (\Lambda_0 q)|_T := \Lambda_0^T q \quad \forall T \in \mathcal{T}_h.$$

It is clear that operator Λ_0 satisfies the approximation property

$$\|v - \Lambda_0 v\|_{0,\Omega} \leq Ch|v|_{1,T} \quad \forall v \in \mathbf{H}^1(\Omega). \quad (5.2)$$

In turn, we can proceed analogously to Section 4.3 of [7] and utilise the trace inequality (4.1) and estimates (5.1) with $m = 1$ and $s = 2$ to obtain the bound

$$\|\mathbf{u} - \mathbf{\Pi}_1 \mathbf{u}\|_h \leq Ch \|\mathbf{u}\|_{2,\Omega} \quad \forall \mathbf{u} \in \mathbf{H}^2(\Omega). \quad (5.3)$$

Let us now recall the Raviart–Thomas interpolation operator $\Pi_{\text{div}} : \mathbf{H}^1(\Omega) \rightarrow \mathbf{Z}_h$, which, given $\boldsymbol{\tau} \in \mathbf{H}^1(\Omega)$, is characterised by the following identities:

$$\int_e (\Pi_{\text{div}}(\boldsymbol{\tau}) \cdot \mathbf{n}) r = \int_e (\boldsymbol{\tau} \cdot \mathbf{n}) r \quad \forall e \in \mathcal{E}_h, \quad \forall r \in P_0(e). \quad (5.4)$$

As a consequence of (5.4), there holds

$$\text{div}(\Pi_{\text{div}}(\boldsymbol{\tau})) = \Lambda_0(\text{div } \boldsymbol{\tau}).$$

In addition, the operator Π_{div} satisfies the following approximation properties (see for instance [29]):

$$\|\boldsymbol{\tau} - \Pi_{\text{div}}(\boldsymbol{\tau})\|_{0,T} \leq c_1 h_T |\boldsymbol{\tau}|_{1,T} \quad \forall T \in \mathcal{T}_h, \quad (5.5)$$

for each $\boldsymbol{\tau} \in \mathbf{H}^1(\Omega)$, and

$$\|\text{div}(\boldsymbol{\tau} - \Pi_{\text{div}}(\boldsymbol{\tau}))\|_{0,T} \leq c_2 h_T |\text{div } \boldsymbol{\tau}|_{1,T} \quad \forall T \in \mathcal{T}_h, \quad (5.6)$$

for each $\boldsymbol{\tau} \in \mathbf{H}^1(\Omega)$, such that $\text{div } \boldsymbol{\tau} \in \mathbf{H}^1(\Omega)$. Combining (5.5) and (5.6) it is clear that the following global estimate holds

$$\|\boldsymbol{\tau} - \Pi_{\text{div}}(\boldsymbol{\tau})\|_{\text{div},\Omega} \leq Ch(|\boldsymbol{\tau}|_{1,\Omega} + |\text{div } \boldsymbol{\tau}|_{1,\Omega}), \quad (5.7)$$

for each $\boldsymbol{\tau} \in \mathbf{H}^1(\Omega)$, such that $\text{div } \boldsymbol{\tau} \in \mathbf{H}^1(\Omega)$. After these preliminary steps we embark in proving optimal error estimates.

Theorem 5.1. *Let $(\mathbf{u}, \phi, \boldsymbol{\sigma}, p)$ and $(\mathbf{u}_h, \phi_h, \boldsymbol{\sigma}_h, p_h)$ be the solutions of (2.6)–(2.9) and (3.1)–(3.4), respectively, and let us assume that $\mathbf{u} \in \mathbf{H}^2(\Omega)$, $\boldsymbol{\sigma} \in \mathbf{H}^1(\Omega)$, $\text{div } \boldsymbol{\sigma} \in \mathbf{H}^1(\Omega)$, and $\phi, p \in \mathbf{H}^1(\Omega)$. Then, there exists a constant $C > 0$ independent of both h and λ , such that*

$$\begin{aligned} \|\mathbf{u} - \mathbf{u}_h\|_h + \|\phi - \phi_h\|_{0,\Omega} + \|\boldsymbol{\sigma} - \boldsymbol{\sigma}_h\|_{\text{div},\Omega} + \|p - p_h\|_{0,\Omega} \\ \leq Ch(\|\mathbf{u}\|_{2,\Omega} + \|\phi\|_{1,\Omega} + \|\boldsymbol{\sigma}\|_{1,\Omega} + \|\text{div } \boldsymbol{\sigma}\|_{1,\Omega} + \|p\|_{1,\Omega}). \end{aligned}$$

Proof. Let $(\mathbf{u}, \phi, \boldsymbol{\sigma}, p)$ and $(\mathbf{u}_h, \phi_h, \boldsymbol{\sigma}_h, p_h)$ be the solutions of (2.6)–(2.9) and (3.1)–(3.4), respectively. In view of the definition of bilinear forms $a_s^h(\cdot, \cdot)$, $b_s^h(\cdot, \cdot)$ and $\tilde{b}_s^h(\cdot, \cdot)$ along with the regularity assumptions on ϕ and \mathbf{u} , i.e., $\phi \in H^1(\Omega)$ and $\mathbf{u} \in \mathbf{H}^2(\Omega)$ (for more details see also [37] and [64]), we can proceed to test (2.1)–(2.4) against suitable functions and to integrate by parts, to obtain the following relations

$$a_s^h(\mathbf{u}, \mathbf{v}_h) + b_s^h(\mathbf{v}_h, \phi) = F(R_h \mathbf{v}_h) \quad \forall \mathbf{v}_h \in \mathbf{H}_h, \quad (5.8)$$

$$\tilde{b}_s^h(\mathbf{u}, \psi_h) - c_s(\phi, \psi_h) + b_{sf}(\psi_h, p) = 0 \quad \forall \psi_h \in \mathbf{Q}_h, \quad (5.9)$$

$$a_f(\boldsymbol{\sigma}, \boldsymbol{\tau}_h) + b_f(\boldsymbol{\tau}_h, p) = G(\boldsymbol{\tau}_h) \quad \forall \boldsymbol{\tau}_h \in \mathbf{Z}_h, \quad (5.10)$$

$$b_{sf}(\phi, q_h) + b_f(\boldsymbol{\sigma}, q_h) - c_f(p, q_h) = H(q_h) \quad \forall q_h \in \mathbf{Q}_h. \quad (5.11)$$

Next, and in order to alleviate the notation in the subsequent analysis, we write $\mathbf{e}_u := \mathbf{u} - \mathbf{u}_h$, $e_\phi := \phi - \phi_h$, $\mathbf{e}_\sigma := \boldsymbol{\sigma} - \boldsymbol{\sigma}_h$ and $e_p := p - p_h$. As usual, we shall then decompose these errors into

$$\mathbf{e}_u = \boldsymbol{\xi}_u + \boldsymbol{\chi}_u, \quad e_\phi = \xi_\phi + \chi_\phi, \quad \mathbf{e}_\sigma = \boldsymbol{\xi}_\sigma + \boldsymbol{\chi}_\sigma \quad \text{and} \quad e_p = \xi_p + \chi_p, \quad (5.12)$$

where

$$\begin{aligned} \boldsymbol{\xi}_u &:= \mathbf{u} - \mathbf{\Pi}_1(\mathbf{u}), & \boldsymbol{\chi}_u &:= \mathbf{\Pi}_1(\mathbf{u}) - \mathbf{u}_h, & \xi_\phi &:= \phi - \Lambda_0(\phi), & \chi_\phi &:= \Lambda_0(\phi) - \phi_h, \\ \boldsymbol{\xi}_\sigma &:= \boldsymbol{\sigma} - \mathbf{\Pi}_{\text{div}}(\boldsymbol{\sigma}), & \boldsymbol{\chi}_\sigma &:= \mathbf{\Pi}_{\text{div}}(\boldsymbol{\sigma}) - \boldsymbol{\sigma}_h, & \xi_p &:= p - \Lambda_0(p), & \chi_p &:= \Lambda_0(p) - p_h. \end{aligned}$$

Then, in what follows we prove that there exists $C > 0$, independent of h and λ , such that

$$\|\boldsymbol{\chi}_u\|_h + \|\chi_\phi\|_{0,\Omega} + \|\boldsymbol{\chi}_\sigma\|_{\text{div},\Omega} + \|\chi_p\|_{0,\Omega} \leq C(\|\boldsymbol{\xi}_u\|_h + \|\xi_\phi\|_{0,\Omega} + \|\boldsymbol{\xi}_\sigma\|_{\text{div},\Omega} + \|\xi_p\|_{0,\Omega}),$$

thus the desired result can be easily obtained from the latter, the triangle inequality and estimates (5.2), (5.3) and (5.7). We notice that on subtracting (3.1)–(3.4) from (5.8) to (5.11), we immediately obtain the following orthogonality property

$$\begin{aligned} a_s^h(\mathbf{e}_u, \mathbf{v}_h) + b_s^h(\mathbf{v}_h, e_\phi) &= 0 & \forall \mathbf{v}_h \in \mathbf{H}_h, \\ \tilde{b}_s^h(\mathbf{e}_u, \psi_h) - c_s(e_\phi, \psi_h) + b_{sf}(\psi_h, e_p) &= 0 & \forall \psi_h \in \mathbf{Q}_h, \\ a_f(\mathbf{e}_\sigma, \boldsymbol{\tau}_h) + b_f(\boldsymbol{\tau}_h, e_p) &= 0 & \forall \boldsymbol{\tau}_h \in \mathbf{Z}_h, \\ b_{sf}(e_\phi, q_h) + b_f(\mathbf{e}_\sigma, q_h) - c_f(e_p, q_h) &= 0 & \forall q_h \in \mathbf{Q}_h, \end{aligned}$$

which, together with the decompositions (5.12), implies that

$$\begin{aligned} a_s^h(\boldsymbol{\chi}_u, \mathbf{v}_h) + b_s^h(\mathbf{v}_h, \chi_\phi) &= F_1^h(\mathbf{v}_h) & \forall \mathbf{v}_h \in \mathbf{H}_h, \\ \tilde{b}_s^h(\boldsymbol{\chi}_u, \psi_h) - c_s(\chi_\phi, \psi_h) + b_{sf}(\psi_h, \chi_p) &= G_1^h(\psi_h) & \forall \psi_h \in \mathbf{Q}_h, \\ a_f(\boldsymbol{\chi}_\sigma, \boldsymbol{\tau}_h) + b_f(\boldsymbol{\tau}_h, \chi_p) &= F_2^h(\boldsymbol{\tau}_h) & \forall \boldsymbol{\tau}_h \in \mathbf{Z}_h, \\ b_{sf}(\chi_\phi, q_h) + b_f(\boldsymbol{\chi}_\sigma, q_h) - c_f(\chi_p, q_h) &= G_2^h(q_h) & \forall q_h \in \mathbf{Q}_h, \end{aligned} \quad (5.13)$$

with

$$\begin{aligned} F_1^h(\mathbf{v}_h) &:= -a_s^h(\boldsymbol{\xi}_u, \mathbf{v}_h) - b_s^h(\mathbf{v}_h, \xi_\phi), & G_1^h(\psi_h) &:= c_s(\xi_\phi, \psi_h) - \tilde{b}_s^h(\boldsymbol{\xi}_u, \psi_h) - b_{sf}(\psi_h, \xi_p), \\ F_2^h(\boldsymbol{\tau}_h) &:= -a_f(\boldsymbol{\xi}_\sigma, \boldsymbol{\tau}_h) - b_f(\boldsymbol{\tau}_h, \xi_p), & G_2^h(q_h) &:= c_f(\xi_p, q_h) - b_{sf}(\xi_\phi, q_h) - b_f(\boldsymbol{\xi}_\sigma, q_h). \end{aligned}$$

Then, applying Theorem 4.1 to (5.13) we deduce that there exists $C > 0$, independent of λ and h , such that

$$\|\boldsymbol{\chi}_u\|_h + \|\chi_\phi\|_{0,\Omega} + \|\boldsymbol{\chi}_\sigma\|_{\text{div},\Omega} + \|\chi_p\|_{0,\Omega} \leq C(\|F_1^h\|_{\mathbf{H}'_h} + \|G_1^h\|_{\mathbf{Q}'_h} + \|F_2^h\|_{\mathbf{Z}'_h} + \|G_2^h\|_{\mathbf{Q}'_h}). \quad (5.14)$$

Now we proceed to bound the norms on the right-hand side of (5.14). We start by observing that from the continuity of a_s^h and b_s^h (cf. (4.2) and (4.7), respectively), we obtain

$$\|F_1^h\|_{\mathbf{H}'_h} \leq c_1(\|\boldsymbol{\xi}_u\|_h + \|\xi_\phi\|_{0,\Omega}),$$

with $c_1 > 0$ independent of λ and h . In turn, using again the continuity of b_s^h , together with the continuity of c_s and b_{sf} (cf. (2.11)), it follows that

$$\|G_1^h\|_{\mathbf{Q}'_h} \leq c_2(\lambda^{-1}\|\xi_\phi\|_{0,\Omega} + \lambda^{-1}\|\xi_p\|_{0,\Omega} + \|\boldsymbol{\xi}_u\|_h),$$

with $c_2 > 0$ independent of λ and h . Next, to bound $\|F_2^h\|_{\mathbf{Z}'_h}$ we make use of the continuity of a_f and b_f (cf. (2.11)) to get

$$\|F_2^h\|_{\mathbf{Z}'_h} \leq c_3(\|\boldsymbol{\xi}_\sigma\|_{\text{div},\Omega} + \|\xi_p\|_{0,\Omega}),$$

with $c_3 > 0$ independent of λ and h . Finally, the continuity of c_f , b_{sf} and b_f (cf. (2.11)) imply

$$\|G_2^h\|_{Q'_h} \leq c_4(\|\xi_p\|_{0,\Omega} + \lambda^{-1}\|\xi_\phi\|_{0,\Omega} + \|\xi_\sigma\|_{\text{div},\Omega}), \quad (5.15)$$

with $c_4 > 0$ independent of λ and h . Therefore, from (5.14) and (5.15) we obtain that there exists $C > 0$, independent of λ and h , such that

$$\|\chi_u\|_h + \|\chi_\phi\|_{0,\Omega} + \|\chi_\sigma\|_{\text{div},\Omega} + \|\chi_p\|_{0,\Omega} \leq C(\|\xi_u\|_h + (1 + 2\lambda^{-1})\|\xi_\phi\|_{0,\Omega} + \|\xi_\sigma\|_{\text{div},\Omega} + (2 + \lambda^{-1})\|\xi_p\|_{0,\Omega}),$$

which combined with the fact that $1 + 2\lambda^{-1}$ and $2 + \lambda^{-1}$ can be seen as constants independent of λ if $\lambda \rightarrow \infty$, concludes the proof. \square

6. NUMERICAL VERIFICATION

We now provide a set of examples serving to illustrate convergence and locking-free properties of the proposed method. In contrast with the computational implementation of conforming FVE schemes (where only mass and source terms need to define matrix blocks that interact with the control volumes in the dual meshes), our coupled DFV-MFE solver uses an explicit construction of the inter-mesh projection map, as the associated interpolation matrix is used in the contributions due to strain and the off-diagonal bilinear forms $b_1^h(\cdot, \cdot)$ and $\tilde{b}_1^h(\cdot, \cdot)$. All operations involving matrix assembly and the solution of linear systems using distributed Krylov solvers, were performed with an in-house code based on the libraries Trilinos (www.trilinos.org) and OpenMPI (www.open-mpi.org), and primal meshes used in Examples 1–4 were generated with GMSH [30].

Example 1: Convergence test and locking phenomenon. In order to experimentally confirm the error estimates derived in Theorem 5.1 we consider a rectangular domain $\Omega = (0, 3/2) \times (0, 1)$, where the boundaries are split as $\Gamma_u = \{(x, y) : x = 0 \text{ or } y = 1\}$ and $\Gamma_p = \{(x, y) : x = 3/2 \text{ or } y = 0\}$. We employ the approach of manufactured solutions and propose the following closed form solutions to (2.1)–(2.4)

$$\mathbf{u} = \begin{pmatrix} -16x^2(x-1)^2y(y-1)(2y-1) + \frac{x^2}{2E\lambda} \\ 16y^2(y-1)^2x(x-1)(2x-1) + \frac{y}{2E\lambda} \end{pmatrix}, \quad p = x^3 - y^4, \quad \phi = \alpha p - \lambda \text{div } \mathbf{u}, \quad \boldsymbol{\sigma} = -\frac{\kappa}{\eta}(\nabla p - \rho \mathbf{g}).$$

These smooth functions are used to construct a body force \mathbf{f} , a fluid source ℓ , the non-homogeneous Dirichlet pressure p_Γ , and a non-homogeneous normal stress defined on Γ_p . The non-dimensional model and discretisation parameters adopted in this test are chosen as follows: $\eta = c_0 = \kappa_0 = 0.001$, $\alpha = \rho = \theta = 1$, $\kappa(\mathbf{x}) = \kappa_0[1 + \kappa_0 \sin^2(\pi x) \cos^2(\pi y)]$, $\mathbf{g} = (0, -1)^T$, and $\gamma_u = 1000$. The Young modulus is $E = 100$, whereas for the Poisson ratio we will consider three cases assigning $\nu = 0.4$ (giving $\mu = 35.71$, $\lambda = 42.857$) $\nu = 0.495$ (with $\mu = 33.44$, $\lambda = 3311.04$), and $\nu = 0.4999$ (implying $\mu = 33.333$, $\lambda = 1.666e4$).

On a sequence of uniformly refined meshes we produce approximate solutions using the proposed DFV-MFE method, and in Table 1 we collect errors computed in the norms suggested by the analysis of Section 5, together with convergence rates calculated as

$$\text{rate} = \log\left(\frac{e(\cdot)}{\hat{e}(\cdot)}\right)[\log(h/\hat{h})]^{-1},$$

where e, \hat{e} stand for errors generated by methods defined on meshes with meshsizes h, \hat{h} , respectively. We can see that the error decay provides verification of the overall first order approximation anticipated by our theoretical results, holding irrespectively of the value of λ . The converged solutions for the intermediate value of the Poisson ratio, are displayed in Figure 2. A similar test is conducted to test the robustness with respect to the specific storage coefficient c_0 , where we fix the Poisson ratio $\nu = 0.495$. Table 2 shows that the convergence rates. As in *e.g.* the test for a single network from [34], the error for three different values of c_0 shows optimal decay. Furthermore, and in contrast with [34], here we also observe that the error magnitude remains unchanged, where all errors are measured for each individual variable in its canonical norm. The linear solves were performed using the BiCGStab method, and the implementation of the non-homogeneous Dirichlet conditions is done *via* Nitsche's approach.

TABLE 1. Test 1. Error history for the DFV-MFE scheme (3.1)–(3.4) approximating the four-field poroelasticity equations for different values of the Poisson ratio.

DoF	h	$\ \mathbf{u} - \mathbf{u}_h\ _{0,\Omega}$		$\ \mathbf{u} - \mathbf{u}_h\ _h$		$\ \phi - \phi_h\ _{0,\Omega}$		$\ \boldsymbol{\sigma} - \boldsymbol{\sigma}_h\ _{0,\Omega}$		$\ \boldsymbol{\sigma} - \boldsymbol{\sigma}_h\ _{\text{div},\Omega}$		$\ p - p_h\ _{0,\Omega}$	
		error	rate	error	rate	error	rate	error	rate	error	rate	error	rate
$\nu = 0.4$													
80	0.78	0.0744	–	0.6926	–	3.6644	–	1.2167	–	2.3256	–	0.3773	–
177	0.52	0.0619	0.45	0.5504	0.57	2.2433	0.69	0.9013	0.74	1.6331	0.87	0.2476	1.04
485	0.31	0.0331	1.22	0.4091	0.58	1.1622	0.84	0.5755	0.88	0.9954	0.97	0.1456	1.04
1557	0.17	0.0133	1.55	0.2559	0.79	0.5785	0.94	0.3296	0.94	0.5581	0.98	0.0799	1.02
5525	0.09	0.0042	1.80	0.1409	0.94	0.3190	0.75	0.1767	0.98	0.2967	0.99	0.0421	1.01
20 757	0.04	0.0012	1.95	0.0734	0.98	0.1665	0.94	0.0914	0.99	0.1531	0.99	0.0217	1.00
80 405	0.02	0.0003	1.98	0.0374	0.99	0.0842	1.00	0.0465	0.99	0.0778	1.00	0.0110	1.00
316 437	0.01	0.0001	1.99	0.0189	1.00	0.0422	1.00	0.0234	1.00	0.0392	1.00	0.0055	1.00
$\nu = 0.495$													
80	0.78	0.0834	–	0.6878	–	5.3694	–	1.2179	–	2.3261	–	0.3774	–
177	0.52	0.0832	0.42	0.5843	0.50	2.4471	0.90	0.9020	0.75	1.6322	0.87	0.2479	1.03
485	0.31	0.0466	1.53	0.4534	0.59	1.6185	0.64	0.5756	0.87	0.9938	0.97	0.1456	1.04
1557	0.17	0.0191	1.61	0.2892	0.76	1.0467	0.65	0.3296	0.94	0.5568	0.98	0.0799	1.02
5525	0.09	0.0062	1.77	0.1606	0.92	0.6353	0.79	0.1767	0.98	0.2959	0.99	0.0421	1.01
20 757	0.04	0.0017	1.96	0.0836	0.98	0.3675	0.83	0.0914	0.99	0.1526	0.99	0.0217	1.00
80 405	0.02	0.0004	2.05	0.0424	1.00	0.1955	0.93	0.0465	0.99	0.0775	1.00	0.0110	1.00
316 437	0.01	0.0001	1.94	0.0213	1.00	0.1051	0.95	0.0234	0.99	0.0391	1.00	0.0055	1.00
$\nu = 0.49999$													
80	0.78	0.1243	–	0.6877	–	6.9456	–	1.2180	–	2.3262	–	0.3774	–
177	0.52	0.0855	0.33	0.5884	0.39	4.8192	0.84	0.9021	0.74	1.6323	0.87	0.2479	1.03
485	0.31	0.0480	1.12	0.4584	0.48	2.7653	0.93	0.5756	0.88	0.9938	0.97	0.1456	1.04
1557	0.17	0.0198	1.51	0.2928	0.76	1.7567	0.92	0.3296	0.95	0.5568	0.98	0.0799	1.02
5525	0.09	0.0065	1.74	0.1630	0.92	0.9291	0.75	0.1767	0.98	0.2959	0.99	0.0421	1.00
20 757	0.04	0.0019	1.91	0.0851	0.98	0.4892	0.86	0.0914	0.99	0.1526	0.99	0.0217	1.00
80 405	0.02	0.0005	2.01	0.0433	0.99	0.2657	0.86	0.0465	0.99	0.0775	1.00	0.0110	1.00
316 437	0.01	0.0001	2.01	0.0218	1.00	0.1632	0.74	0.0234	1.00	0.0391	1.00	0.0055	1.00

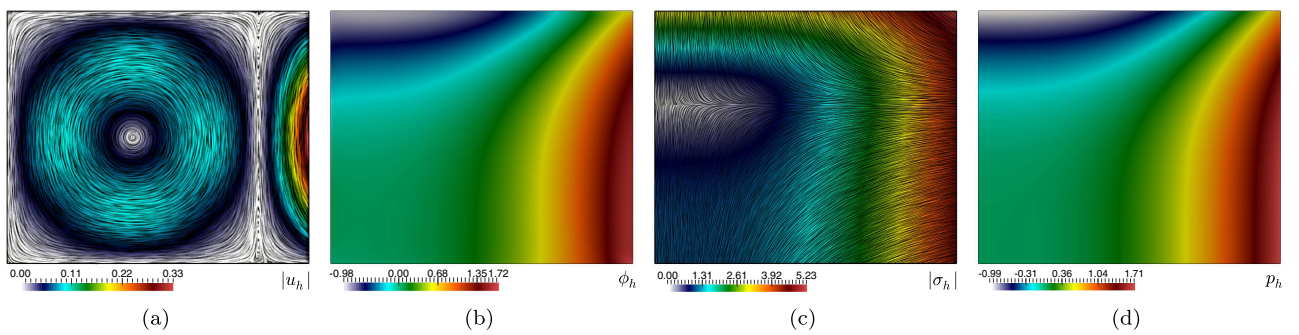


FIGURE 2. Test 1. Approximate displacement magnitude (a), total pressure (b), fluid flux (c), and fluid pressure (c); computed for $\mu = 33.44$, $\lambda = 3311.04$, on a mesh with 33 282 primal elements.

TABLE 2. Test 1. Error history for the DFV-MFE scheme (3.1)–(3.4) approximating the four-field poroelasticity equations for different values of the specific storage coefficient.

DoF	h	$\ \mathbf{u} - \mathbf{u}_h\ _{0,\Omega}$		$\ \mathbf{u} - \mathbf{u}_h\ _h$		$\ \phi - \phi_h\ _{0,\Omega}$		$\ \boldsymbol{\sigma} - \boldsymbol{\sigma}_h\ _{0,\Omega}$		$\ \boldsymbol{\sigma} - \boldsymbol{\sigma}_h\ _{\text{div},\Omega}$		$\ p - p_h\ _{0,\Omega}$	
		error	rate	error	rate	error	rate	error	rate	error	rate	error	rate
$c_0 = 1$													
80	0.78	0.0768	–	0.7066	–	2.3261	–	1.2064	–	2.3230	–	0.3746	–
177	0.52	0.0525	0.93	0.5356	0.68	1.8007	0.43	0.8971	0.73	1.6308	0.87	0.2469	1.02
485	0.31	0.0281	1.22	0.3819	0.66	1.3222	0.61	0.5743	0.87	0.9934	0.97	0.1454	1.03
1557	0.17	0.0115	1.52	0.2318	0.84	0.8793	0.69	0.3294	0.94	0.5567	0.98	0.0799	1.01
5525	0.09	0.0036	1.81	0.1260	0.95	0.4183	1.16	0.1766	0.97	0.2959	0.99	0.0421	1.00
20757	0.04	0.0010	1.95	0.0655	0.98	0.1715	1.34	0.0914	0.99	0.1526	0.99	0.0217	1.00
$c_0 = 1e-4$													
80	0.78	0.0768	–	0.7066	–	2.3261	–	1.2180	–	2.3261	–	0.3774	–
177	0.52	0.0525	0.94	0.5356	0.68	1.8007	0.43	0.9021	0.74	1.6323	0.87	0.2479	1.03
485	0.31	0.0281	1.22	0.3819	0.66	1.3221	0.61	0.5756	0.87	0.9938	0.97	0.1456	1.04
1557	0.17	0.0115	1.52	0.2318	0.84	0.8793	0.69	0.3296	0.94	0.5568	0.98	0.0799	1.02
5525	0.09	0.0036	1.81	0.1260	0.95	0.4183	1.16	0.1767	0.98	0.2959	0.99	0.0421	1.00
20757	0.04	0.0010	1.95	0.0655	0.98	0.1715	1.34	0.0914	0.99	0.1526	0.99	0.0217	1.00
$c_0 = 0$													
80	0.78	0.0768	–	0.7066	–	2.3261	–	1.2180	–	2.3261	–	0.3774	–
177	0.52	0.0525	0.93	0.5356	0.68	1.8007	0.43	0.9021	0.74	1.6323	0.87	0.2479	1.03
485	0.31	0.0281	1.22	0.3819	0.66	1.3221	0.61	0.5756	0.87	0.9938	0.97	0.1456	1.04
1557	0.17	0.0115	1.52	0.2318	0.84	0.8793	0.69	0.3296	0.94	0.5568	0.98	0.0799	1.02
5525	0.09	0.0036	1.81	0.1260	0.95	0.4183	1.16	0.1767	0.98	0.2959	0.99	0.0421	1.00
20757	0.04	0.0010	1.94	0.0655	0.98	0.1715	1.34	0.0914	0.99	0.1526	0.99	0.0217	1.00

Example 2: Surface footing. We next address the numerical solution of a partial compression problem in 3D. One seeks to determine the deformation as well as the undrained response of the fluid (flux and pressure distribution) of a porous material when subject to a distributed boundary load of magnitude 10 000. The computational domain occupied by the porous medium is a box whose left, right, back and front faces are defined by $x = -100, x = 100, y = 100, y = -100$, while the top and bottom surfaces are defined by the parameterisation

$$t \mapsto z(x, y, t) = 12 \cos(0.01[x + \pi y]) \cos^2(0.01[\pi x + y]) + \frac{1}{4}t + \frac{1}{12}(0.01y - 1), \quad t \in [-100, 100],$$

(as used for a related test in *e.g.* [32]). Its boundary is separated into Ω_{Γ_u} and Ω_{Γ_p} . The former contains portions of the boundary corresponding to the faces $y = -100, y = 100$ and $x = 100$, where we will prescribe zero displacements $\mathbf{u} = \mathbf{0}$ and zero normal fluid flux $\boldsymbol{\sigma} \cdot \mathbf{n} = 0$. On the remainder of $\partial\Omega$ we set zero fluid pressure $p_\Gamma = 0$, and assume a non-homogeneous total normal stress

$$\mathbf{h}_\Gamma = \begin{cases} (10000, 0, 0)^T & \text{if } x = -100 \text{ and } -50 \leq y \leq 50, \\ 0 & \text{otherwise,} \end{cases}$$

imposed according to the condition $(2\mu\boldsymbol{\varepsilon}(\mathbf{u}) - \phi\mathbf{I}) = \mathbf{h}_\Gamma$, on Ω_{Γ_p} . In addition we consider a null source $\mathbf{f} = \mathbf{0}$, a constant fluid source $\ell = 0.01$, the gravity force $\mathbf{g} = (0, 0, -9.8)^T$, Young and Poisson elastic moduli $E = 30\,000$, $\nu = 0.475$, storage and Biot-Willis coefficients $c_0 = 0.001$, $\alpha = 0.1$, permeability of the porous matrix $\kappa = 0.0001$, fluid viscosity $\eta = 0.01$, and fluid density $\rho = 500$. The primal mesh contains 49 152 tetrahedral elements and we take the penalisation parameters $\gamma_u = 100$, together with the symmetric version of the interior penalty method (*i.e.* $\theta = 1$).

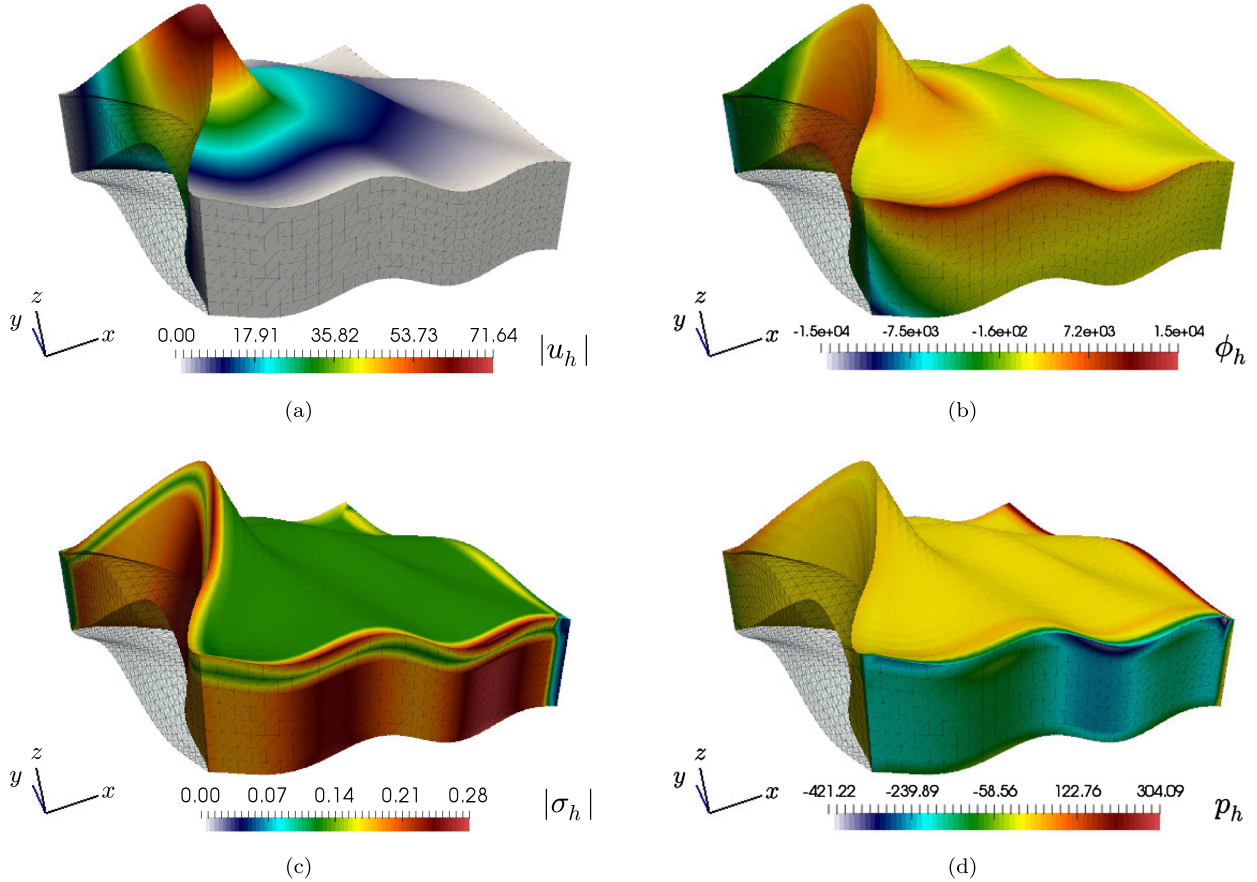


FIGURE 3. Test 2. Deformation and filtration response of a porous block subjected to a normal boundary force at one end. Displacement magnitude (a), total pressure distribution (b), fluid flux (c), and fluid pressure (d).

The obtained approximate solutions are depicted in Figure 3, and rendered on the deformed domain. We also show the undeformed skeleton mesh in each panel. For this test (as well as for test 4 below) we have used a GMRES solver with a tolerance of 10^{-6} , and preconditioned by an ILU factorisation.

Example 3: Loading of a cylindrical shell. For this test we study a transient problem where (2.4) adopts the form

$$\frac{\partial}{\partial t} \left[\left(c_0 + \frac{\alpha^2}{\lambda} \right) p - \frac{\alpha}{\lambda} \phi \right] + \operatorname{div} \boldsymbol{\sigma} = \ell \quad \text{in } \Omega \times (0, T_{\text{final}}), \quad (6.1)$$

where $t \in (0, T)$ denotes the time variable and $T_{\text{final}} = 10^{-5}$ is the final time. As in [1] we consider a 2D domain (a ring of external radius 1 and internal radius 0.5) representing the cross-section of a cylindrical shell made of a deformable porous material. The outer circle will be considered as Γ_u so we impose the domain to be clamped and the normal flux of the fluid pressure is zero. On the inner circle, Γ_p , we impose a fixed fluid pressure $p_\Gamma = 1$ and an *effective solid stress*

$$[2\mu\boldsymbol{\varepsilon}(\boldsymbol{u}) + \lambda(\operatorname{div} \boldsymbol{u})\mathbf{I}]\mathbf{n} = -(\cos(\theta), \sin(\theta))^T,$$

where θ is the second polar coordinate. This implies that the total traction load to impose at Γ_p is $-(\cos(\theta), \sin(\theta)) - p_\Gamma$. We assume the absence of gravitational forces, $\mathbf{g} = \mathbf{0}$, and we take a zero specific storage $c_0 = 0$.

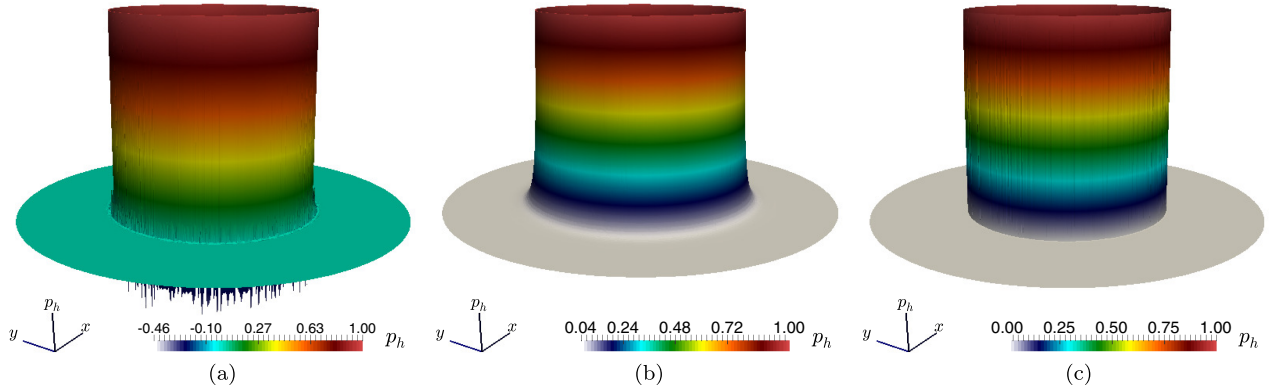


FIGURE 4. Test 3. Transient loading of a cylindrical shell. Snapshot taken at $T_{\text{final}} = 10\Delta t$. Elevation plots according to the fluid pressure computed with: a primal conforming piecewise linear approximation of solid displacement and pressure (a), adding a model stabilisation $-\beta\Delta[\frac{\partial}{\partial t}p]$ with $\beta = h^2/(4\lambda + 8\mu)$ (b), and with the proposed mixed-mixed formulation (c).

Such a configuration is of particular importance as low values of the specific storage have been reported to induce volumetric locking. Even if our theoretical analysis does not support this limit case (see comment at the end of Sect. 2), as we have seen in Table 2 and as will observe below, the proposed mixed-mixed formulation presents no issues associated with $c_0 = 0$. The remaining model parameters take on the following values $E = 10^5$, $\nu = 0.2$, $\alpha = 1$, $\kappa = 10^{-7}$, $\eta = 10^{-3}$. The primal mesh contains 37 084 triangular elements, and the time discretisation of the problem follows a classical backward Euler scheme with a fixed timestep $\Delta t = 10^{-6}$. The stabilisation constant is set as $\gamma_u = 10$ and again we adopt a symmetric interior penalty method.

The model and methods in [1] suggest to incorporate a stabilisation term $-\beta\Delta[\frac{\partial}{\partial t}p]$ on the left hand side of (6.1), with $\beta > 0$ depending on the Lamé constants and the meshsize. We perform a comparison against a conforming discretisation of the Biot consolidation problem formulated solely in terms of solid displacement and fluid pressure, using piecewise linear and continuous Lagrange finite elements for \mathbf{u} and p , and incorporating $\beta = h^2/(4\lambda + 8\mu)$. We observe that such a stabilisation (targeted to eliminate oscillations near the inner boundary Γ_p) generates a marked smoothing of the fluid pressure profile, which is not necessarily consistent with the expected physical behaviour. We also mention that this stabilisation is actually not required in our mixed-mixed method, due to the conservative character of the scheme and its suitability for handling discontinuities and high gradients. The obtained results are displayed in Figure 4. Note that for this transient simulation our theoretical analysis is not valid. Nevertheless the qualitative behaviour of the results indicates that all computations remain stable.

Example 4: A two-layered porous material. We now simulate the drainage behaviour of a porous region composed of two layers with different material properties determined by the discontinuous Lamé moduli of dilation and shear, and the solid permeability

$$\lambda = \mu = \begin{cases} 1e4 & \text{in } \Omega_{\text{bot}}, \\ 1 & \text{in } \Omega_{\text{top}}, \end{cases}, \quad \kappa = \begin{cases} 0.1 & \text{in } \Omega_{\text{bot}}, \\ 10^{-4} & \text{in } \Omega_{\text{top}}, \end{cases}$$

where $\Omega = (0, 1)^3 = \Omega_{\text{bot}} \cup \Omega_{\text{top}}$ with the two subdomains being separated by the plane $z = 0.5$. The solid matrix in the upper domain is softer and less permeable than the material occupying the bottom layer (see a similar test performed in [46]). The constants dictating the hydromechanical coupling (that is, the specific storage and Biot-Willis parameter) are specified as $c_0 = 0.009$, $\alpha = 1$, and the remaining data are $\eta = 1$, $\gamma_u = 100$.

As in Example 2 above, the onset of motion and flow is induced by applying a normal surface load on a part of the boundary. We now use a load of magnitude 5 applied on a disk of centre $(1/4, 1/4, 1)$ and radius 0.2, lying on the top lid. The remainder of the top face, together with the whole bottom square and the faces $x = 0$ and $y = 0$ constitute Γ_p (where the fluid pressure is set to zero and the fluid content is free to drain), whereas we assume that the two remaining lateral walls, defined by $x = 1$ and $y = 1$, are completely rigid and impermeable (on this boundary part, Γ_u , we impose zero displacements and zero normal fluid flux). The domain configuration and the boundary labels are sketched in Figure 5. We took a uniform mesh having 345'600 tetrahedral elements in the primal mesh, resulting in a linear system of 5'538'560 unknowns.

Snapshots of the solutions computed using the proposed DFV-MFE scheme are shown in Figure 5, exhibiting a qualitative agreement with the results from [46]. In particular, the produced approximations do not present spurious oscillations in the computed total and fluid pressures, nor unphysically small displacements. We can also observe that the pressure distributions form an interior boundary layer, but these high gradients do not pollute the numerical approximation.

Example 5: Filtration of cerebro-spinal fluid within brain tissue. We finalise the numerical tests by simulating the filtration process of cerebro-spinal fluid (CSF) due to pressure differences in the brain. The problem setting assumes that the parenchyma is a porous medium fully saturated with CSF, and that the tissue is nearly incompressible, and that no gravitational effects influence the poromechanical dynamics. Model parameters were taken from [40, 58, 60] and are as follows

$$\nu = 0.4999, \quad E = 1500 \text{ Pa}, \quad c_0 = 3.9 \text{ e-4 Pa}^{-1}, \quad \alpha = 0.49, \quad \frac{\kappa}{\eta} = 1.573 \text{ e-5 mm}^2 \text{ Pa}^{-1} \text{ s}^{-1}.$$

The problem adopts again the time-dependent form (6.1) and we use the initial conditions $\phi(0) = 0$, $p(0) = 5 \text{ mmHg}$. A backward Euler scheme is applied using a timestep $\Delta t = 0.025 \text{ s}$ and the system is run for two pulsating cycles, up to $t = 1 \text{ s}$. This model does not consider anisotropy of permeability nor inhomogeneity of fluid content. The domain consists of an adult human brain atlas [26] and we employ a tetrahedral mesh having 29 037 vertices. The boundary conditions differ from (2.5). On Γ_s (the outer surface of the brain which in contact with the skull) we impose $\mathbf{u} = \mathbf{0}$ and a pulsating CSF pressure profile $p_s(t) = p(0) + 2 \sin(2\pi t) \text{ mmHg}$. On the remainder of the boundary (constituted by the ventricles), $\Gamma_v = \partial\Omega \setminus \Gamma_s$, we prescribe a different pulsating pressure having a slightly larger amplitude $p_v(t) = p(0) + 2.016 \sin(2\pi t) \text{ mmHg}$, together with a zero-traction condition $(2\mu\boldsymbol{\varepsilon}(\mathbf{u}) - \phi\mathbf{I})\mathbf{n} = \mathbf{0}$ (implying that the ventricles can deform freely). On the other hand, the total pressure and the fluid flux are not constrained on the boundary. Note that initial and boundary conditions for CSF pressure need to be rescaled from mmHg to Pa. The results collected in Figure 6 are shown after the first cycle, at $t = 0.5 \text{ s}$ and they show qualitative agreement with the displacement and extracellular pressure as reported in Section 6 of [40], however the magnitudes do not match as the model in that reference is much more complete than the one treated here.

7. SUMMARY AND CONCLUDING REMARKS

We have introduced a new mixed-mixed formulation for linear poroelasticity using the total pressure and the fluid flux as additional mixed variables. The proposed discretisation consisted on a combined discontinuous finite volume scheme for the displacement of the solid skeleton, and a mixed finite element method approximating the remaining fields. The method features conservativity, absence of spurious pressure oscillations, and locking free properties. We have derived theoretical error estimates and have confirmed them experimentally through a series of numerical tests in 2D and 3D.

As an extension to this work we foresee the development of high-order discretisations for displacements and total pressure. This is fairly standard for the mixed finite element components of the method, however the discontinuous finite volume part would require much more care, since the structural connection between discontinuous finite volumes and classical DG methods does no longer hold (see for instance the recent paper [22] addressing second order finite volume element schemes for Stokes equations or [23] for Biot's consolidation

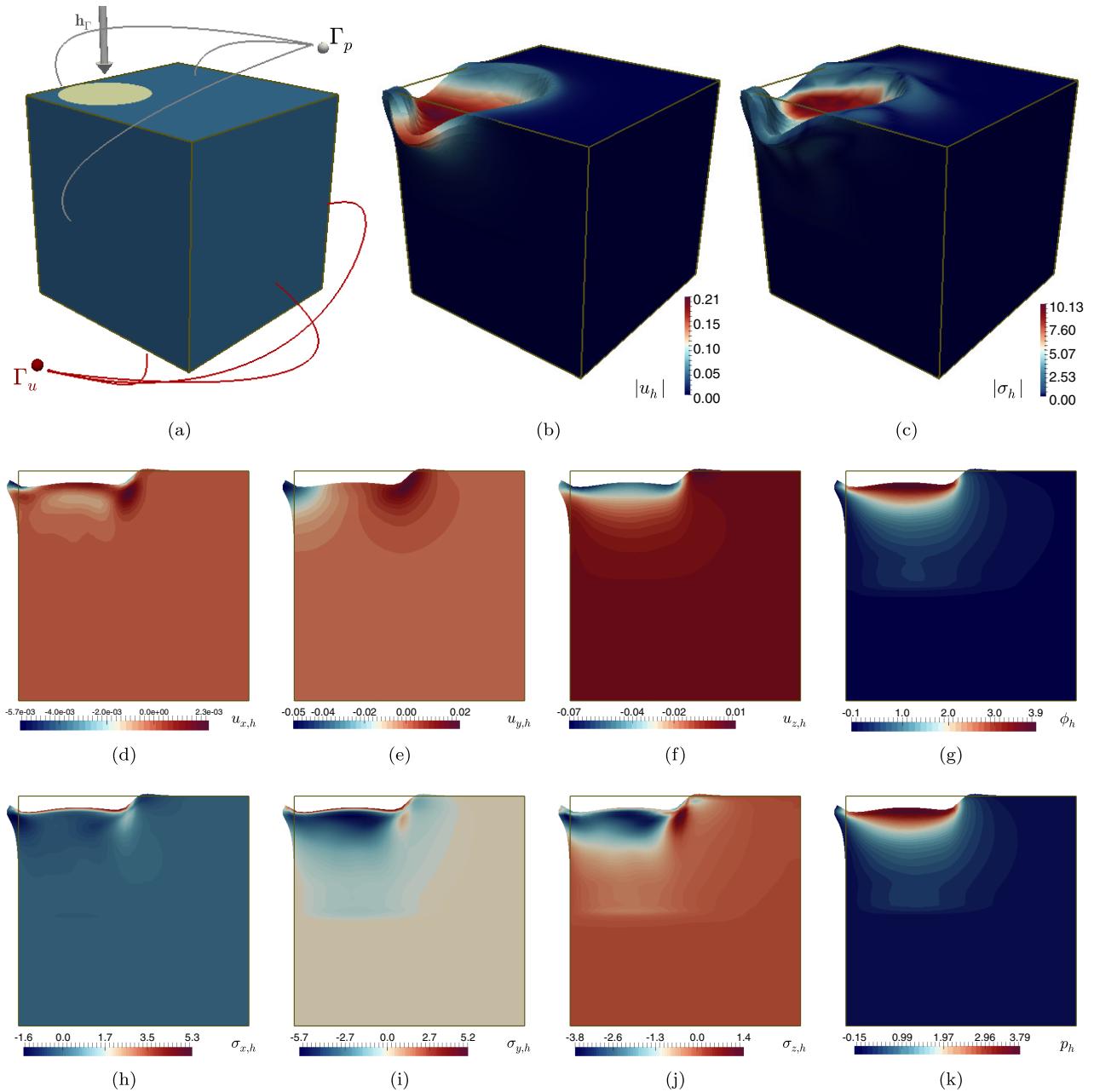


FIGURE 5. Test 4. Deformation and filtration response of a two-layered medium. Sketch of the domain configuration and boundary conditions (a), displacement magnitude (b), fluid flux (c); and snapshots of each scalar field on the slice $x = 0.25$ (d–k).

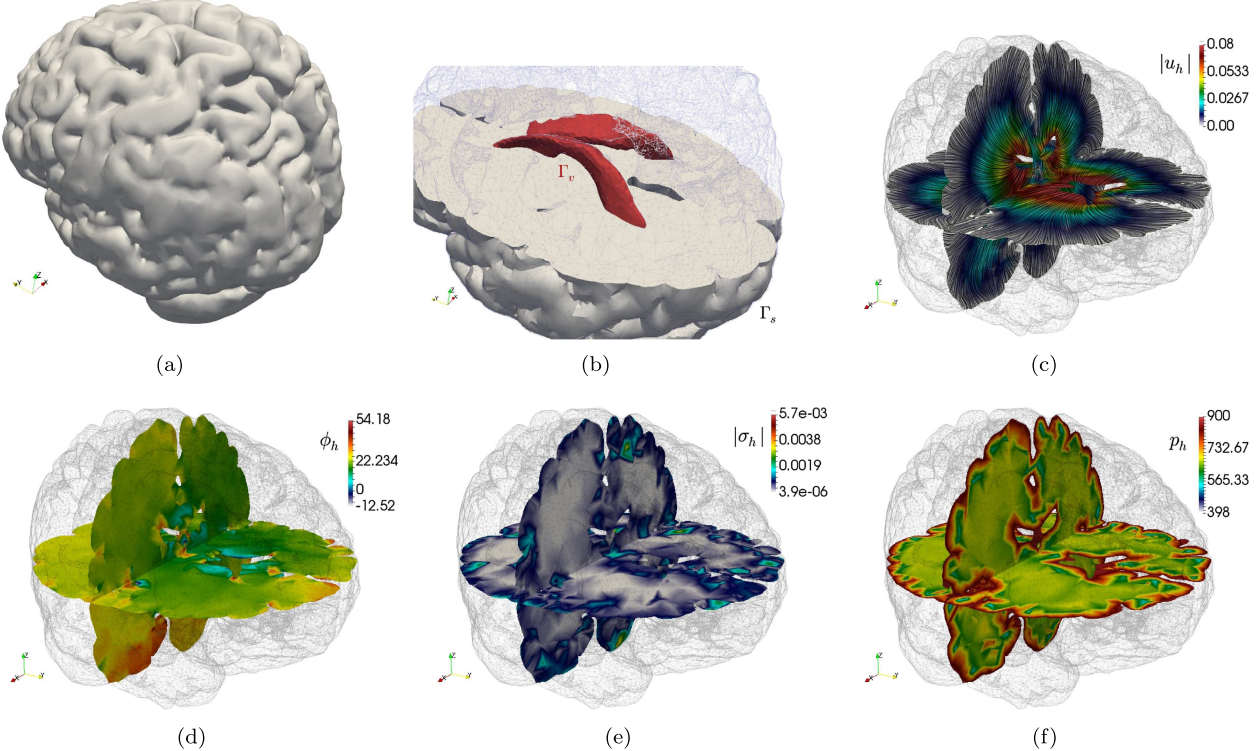


FIGURE 6. Test 5. Geometry from an adult human brain atlas (a), ventricle boundary Γ_v and skull boundary Γ_s (b), and approximate solutions of the Biot equations visualised on slices parallel to the y and z axes, corresponding to the time $t = 0.5$ s. Displacement magnitude and directions line integration contours (c), total pressure (d), magnitude of CSF flux (e), and CSF pressure (f).

in primal formulation). Note that the optimal error estimates found in our analysis demand global regularity of the exact solutions, which does not hold in many instances, including Example 4. Nevertheless, if the mesh is compatible with the discontinuity one may achieve higher regularity, locally. Even if the method does seem to perform well under these conditions, as evidenced by the results of Example 4 (where it can be seen that the computed solutions do not show spurious oscillations); a more delicate theoretical analysis is required. A further step would be to derive a posteriori error estimates, focusing on the zones of fluid singularities and stress concentration [52]. Moreover, recent extensions of robust and efficient schemes for Biot equations have been employed for the more sophisticated model of multiple network poroelasticity in *e.g.* [34, 40, 60], or to the case of coupled poromechanics and advection–diffusion [48, 49, 51, 56], and we are extending our formulation to accommodate those cases as well. We would also like to investigate fractures and energy conservation aspects as recently addressed in [16], as well as the generalisation of our theoretical and computational framework (presently confined to the linear case) to the study of interface problems [4], also including the regime of finite strains [11, 20, 61]. We finally mention that large scale problems will require the design of suitable preconditioners, for which we can appeal to the recent developments in *e.g.* [9, 34, 39].

Acknowledgements. This research has been partially supported by the London Mathematical Society through the research grant Scheme 5 – 51703; and by CONICYT-Chile through project Fondecyt 1161325 and project AFB170001 of the PIA Program: Concurso Apoyo a Centros Científicos y Tecnológicos de Excelencia con Financiamiento Basal. We thank the

thorough work of two anonymous referees whose suggestions and constructive criticism lead to a number of improvements with respect to the initial version of this manuscript. We also thank Eleonora Persanti, Matteo Croci, Marie E. Rognes, and Kent-André Mardal for providing the human brain geometry and all relevant model parameters employed in Test 5.

REFERENCES

- [1] F. Aguilar, F.L. Gaspar and C. Rodrigo, Numerical stabilization of Biot's consolidation model by a perturbation on the flow equation. *Int. J. Numer. Methods Eng.* **75** (2008) 1282–1300.
- [2] E. Ahmed, F.A. Radu and J.M. Nordbotten, Adaptive poromechanics computations based on a posteriori error estimates for fully mixed formulations of Biot's consolidation model. *Comput. Methods Appl. Mech. Eng.* **347** (2019) 264–294.
- [3] I. Ambartsumyan, E. Khattatov, I. Yotov and P. Zunino, A Lagrange multiplier method for a Stokes–Biot fluid-poroelastic structure interaction model. *Numer. Math.* **140** (2018) 513–553.
- [4] V. Anaya, Z. De Wijn, B. Gómez-Vargas, D. Mora and R. Ruiz-Baier, Rotation-based mixed formulations for an elasticity-poroelasticity interface problem. Submitted preprint (2019). Available from <https://www.ci2ma.udec.cl/publicaciones/prepublicaciones/>.
- [5] V. Anaya, Z. De Wijn, D. Mora and R. Ruiz-Baier, Mixed displacement-rotation-pressure formulations for linear elasticity. *Comput. Methods Appl. Mech. Eng.* **344** (2019) 71–94.
- [6] D.N. Arnold, An interior penalty finite element method with discontinuous elements. *SIAM J. Numer. Anal.* **19** (1982) 742–760.
- [7] D.N. Arnold, F. Brezzi, B. Cockburn and L.D. Marini, Unified analysis of discontinuous Galerkin methods for elliptic problems. *SIAM J. Numer. Anal.* **39** (2002) 1749–1779.
- [8] R. Asadi, B. Ataie-Ashtiani and C.T. Simmons, Finite volume coupling strategies for the solution of a Biot consolidation model. *Comput. Geotech.* **55** (2014) 494–505.
- [9] T. Bærland, J.J. Lee, K.-A. Mardal and R. Winther, Weakly imposed symmetry and robust preconditioners for Biot's consolidation model. *Comput. Methods Appl. Math.* **17** (2017) 377–396.
- [10] L. Berger, R. Bordas, D. Kay and S. Tavener, Stabilized lowest-order finite element approximation for linear three-field poroelasticity. *SIAM J. Sci. Comput.* **37** (2015) A2222–A2245.
- [11] L. Berger, R. Bordas, D. Kay and S. Tavener, A stabilized finite element method for finite-strain three-field poroelasticity. *Comput. Mech.* **60** (2017) 51–68.
- [12] M.A. Biot, Theory of elasticity and consolidation for a porous anisotropic solid. *J. Appl. Phys.* **26** (1955) 182–185.
- [13] D. Boffi, M. Botti and D.A. Di Pietro, A nonconforming high-order method for the Biot problem on general meshes. *SIAM J. Sci. Comput.* **38** (2016) A1508–A1537.
- [14] D. Boffi, F. Brezzi and M. Fortin, Mixed finite element methods and applications. In: Vol. 44 of *Springer Series in Computational Mathematics*. Springer (2010).
- [15] H. Brezis, Functional Analysis, Sobolev Spaces and Partial Differential Equations. Springer Verlag (2010).
- [16] M. Bukač, I. Yotov and P. Zunino, Dimensional model reduction for flow through fractures in poroelastic media. *ESAIM: M2AN* **51** (2017) 1429–1471.
- [17] R. Bürger, S. Kumar and R. Ruiz-Baier, Discontinuous finite volume element discretization for coupled flow-transport problems arising in models of sedimentation. *J. Comput. Phys.* **299** (2015) 446–471.
- [18] C. Carstensen, N. Nataraj and A.K. Pani, Comparison results and unified analysis for first-order finite volume element methods for a Poisson model problem. *IMA J. Numer. Anal.* **36** (2016) 1120–1142.
- [19] N. Castelletto, J.A. White and M. Ferronato, Scalable algorithms for three-field mixed finite element coupled poromechanics. *J. Comput. Phys.* **327** (2016) 894–918.
- [20] D. Chapelle and P. Moireau, General coupling of porous flows and hyperelastic formulations – From thermodynamics principles to energy balance and compatible time schemes. *Eur. J. Mech. B/Fluids* **46** (2014) 82–96.
- [21] Y. Chen, Y. Luo and M. Feng, Analysis of a discontinuous Galerkin method for the Biot's consolidation problem. *Appl. Math. Comput.* **219** (2013) 9043–9056.
- [22] Z. Chen, Y. Xu and Y. Zhang, A second-order hybrid finite volume method for solving the Stokes equation. *Appl. Numer. Math.* **119** (2017) 213–224.
- [23] Z. De Wijn, R. Oyarzúa and R. Ruiz-Baier, A second-order finite-volume-element scheme for linear poroelasticity. Submitted preprint (2019). Available from <https://www.ci2ma.udec.cl/publicaciones/prepublicaciones/>.
- [24] Q. Deng, V. Ginting, B. McCaskill and P. Torsu, A locally conservative stabilized continuous Galerkin finite element method for two-phase flow in poroelastic subsurfaces. *J. Comput. Phys.* **347** (2017) 78–98.
- [25] D. Di Pietro and A. Ern, Mathematical aspects of discontinuous Galerkin methods. In: Vol. 69 of *Mathématiques & Applications*. Springer, Heidelberg (2012).
- [26] Q. Fang and D.A. Boas, Monte Carlo simulation of photon migration in 3D turbid media accelerated by graphics processing units. *Opt. Express* **17** (2009) 20178–20190.
- [27] X. Feng, Z. Ge and Y. Li, Analysis of a multiphysics finite element method for a poroelasticity model. *IMA J. Numer. Anal.* **38** (2018) 330–359.
- [28] G. Fu, A high-order HDG method for the Biot's consolidation model. *Comput. Math. Appl.* **77** (2019) 237–252.
- [29] G.N. Gatica, A Simple Introduction to the Mixed Finite Element Method. Theory and Applications. *Springer Briefs in Mathematics*. Springer, Cham (2014).

- [30] C. Geuzaine and J.-F. Remacle, Gmsh: a three-dimensional finite element mesh generator with built-in pre- and post-processing facilities. *Int. J. Numer. Methods Eng.* **79**(11) (2009) 1309–1331.
- [31] V. Girault and P.-A. Raviart, Finite element approximation of the Navier–Stokes equations. In: Vol. 749 of *Lecture Notes in Mathematics*. Springer-Verlag, Berlin–New York (1979).
- [32] V. Girault, M.F. Wheeler, B. Ganis and M.E. Mear, A lubrication fracture model in a poro-elastic medium. *Math. Models Methods Appl. Sci.* **25** (2015) 587–645.
- [33] Q. Hong and J. Kraus, Parameter-robust stability of classical three-field formulation of Biot’s consolidation model. *Electron. Trans. Numer. Anal.* **48** (2018) 202–226.
- [34] Q. Hong, J. Kraus, M. Lymbery and F. Philo, Conservative discretizations and parameter-robust preconditioners for Biot and multiple-network flux-based poroelasticity models. *Numer. Linear Alg. Appl.* **26** (2019) e2242.
- [35] X. Hu, C. Rodrigo, F.J. Gaspar and L.T. Zikatanov, A non-conforming finite element method for the Biot’s consolidation model in poroelasticity. *J. Comput. Appl. Math.* **310** (2017) 143–154.
- [36] G. Kanschat and B. Rivière, A finite element method with strong mass conservation for Biot’s linear consolidation model. *J. Sci. Comput.* **77** (2018) 1762–1779.
- [37] S. Kumar and R. Ruiz-Baier, Equal order discontinuous finite volume element methods for the Stokes problem. *J. Sci. Comput.* **65** (2015) 956–978.
- [38] R. Lazarov and X. Ye, Stabilized discontinuous finite element approximations for Stokes equations. *J. Comput. Appl. Math.* **198** (2007) 236–252.
- [39] J.J. Lee, K.-A. Mardal and R. Winther, Parameter-robust discretization and preconditioning of Biot’s consolidation model. *SIAM J. Sci. Comput.* **39** (2017) A1–A24.
- [40] J.J. Lee, E. Persanti, K.-A. Mardal and M.E. Rognes, A mixed finite element method for nearly incompressible multiple-network poroelasticity. *SIAM J. Sci. Comput.* **41** (2019) A722–A747.
- [41] R.W. Lewis and B.A. Schrefler, The Finite Element Method in the Deformation of and Consolidation of Porous Media. Wiley & Sons, Chichester (1987).
- [42] R. Liu, M.F. Wheeler, C.N. Dawson and R.H. Dean, On a coupled discontinuous/continuous Galerkin framework and an adaptive penalty scheme for poroelasticity problems. *Comput. Methods Appl. Mech. Eng.* **198** (2009) 3499–3510.
- [43] K.-A. Mardal and R. Winther, Preconditioning discretizations of systems of partial differential equations. *Numer. Linear Algebra Appl.* **18** (2011) 1–40.
- [44] M.A. Murad, V. Thomée and A.F.D. Loula, Asymptotic behavior of semi discrete finite-element approximations of Biot’s consolidation problem. *SIAM J. Numer. Anal.* **33** (1996) 1065–1083.
- [45] A. Naumovich, On finite volume discretization of the three-dimensional Biot poroelasticity system in multilayer domains. *Comput. Methods Appl. Math.* **6** (2006) 306–325.
- [46] A. Naumovich and F.J. Gaspar, On a multigrid solver for the three-dimensional Biot poroelasticity system in multilayered domains. *Comput. Vis. Sci.* **11** (2008) 77–87.
- [47] R. Oyarzúa and R. Ruiz-Baier, Locking-free finite element methods for poroelasticity. *SIAM J. Numer. Anal.* **54** (2016) 2951–2973.
- [48] R. Penta, D. Ambrosi and R.J. Shipley, Effective governing equations for poroelastic growing media. *Q. J. Mech. Appl. Math.* **67** (2014) 69–91.
- [49] G.P. Peters and D.W. Smith, Solute transport through a deforming porous medium. *Int. J. Numer. Anal. Methods Geomech.* **26** (2002) 683–717.
- [50] P.J. Phillips and M.F. Wheeler, A coupling of mixed and discontinuous Galerkin finite-element methods for poroelasticity. *Comput. Geosci.* **12** (2008) 417–435.
- [51] M. Radzuweit, H. Engel and M. Bär, An active poroelastic model for mechanochemical patterns in protoplasmic droplets of physarum polycephalum. *PLoS One* **9** (2014) e99220.
- [52] R. Riedlbeck, D.A. Di Pietro, A. Ern, S. Granet and K. Kazymyrenko, Stress and flux reconstruction in Biot’s poro-elasticity problem with application to a posteriori error analysis. *Comput. Math. Appl.* **73** (2017) 1593–1610.
- [53] B. Rivière, J. Tan and T. Thompson, Error analysis of primal discontinuous Galerkin methods for a mixed formulation of the Biot equations. *Comput. Math. Appl.* **73** (2017) 666–683.
- [54] C. Rodrigo, F.J. Gaspar, X. Hu and L.T. Zikatanov, Stability and monotonicity for some discretizations of the Biot’s consolidation model. *Comput. Methods Appl. Mech. Eng.* **298** (2016) 183–204.
- [55] R. Ruiz-Baier and I. Lunati, Mixed finite element – discontinuous finite volume element discretization of a general class of multicontinuum models. *J. Comput. Phys.* **322** (2016) 666–688.
- [56] R. Sacco, P. Causin, C. Lelli and M.T. Raimondi, A poroelastic mixture model of mechanobiological processes in biomass growth: theory and application to tissue engineering. *Meccanica* **52** (2017) 3273–3297.
- [57] R.E. Showalter, Diffusion in poro-elastic media. *J. Math. Anal. Appl.* **251** (2000) 310–340.
- [58] K.H. Støverud, M. Alnæs, H.P. Langtangen, V. Haughton and K.-A. Mardal, Poro-elastic modeling of Syringomyelia – a systematic study of the effects of pia mater, central canal, median fissure, white and gray matter on pressure wave propagation and fluid movement within the cervical spinal cord. *Comput. Methods Biomed. Eng.* **19** (2016) 686–698.
- [59] M. Sun and H. Rui, A coupling of weak Galerkin and mixed finite element methods for poroelasticity. *Comput. Math. Appl.* **73** (2017) 804–823.
- [60] J.C. Vardakas, D. Chou, B.J. Tully, C.C. Hung, T.H. Lee, P.-H. Tsui and Y. Ventikos, Investigating cerebral oedema using poroelasticity. *Med. Eng. Phys.* **38** (2016) 48–57.

- [61] A.-T. Vuong, L. Yoshihara and W.A. Wall, A general approach for modeling interacting flow through porous media under finite deformations. *Comput. Methods Appl. Mech. Eng.* **283** (2015) 1240–1259.
- [62] M.F. Wheeler, G. Xue and I. Yotov, Coupling multipoint flux mixed finite element methods with continuous Galerkin methods for poroelasticity. *Comput. Geosci.* **18** (2014) 57–75.
- [63] J.A. White and R.I. Borja, Stabilized low-order finite elements for coupled solid-deformation/fluid-diffusion and their application to fault zone transients. *Comput. Methods Appl. Mech. Eng.* **197** (2008) 4353–4366.
- [64] X. Ye, A discontinuous finite volume method for the Stokes problem. *SIAM J. Numer. Anal.* **44** (2006) 183–198.
- [65] S.-Y. Yi, A Coupling of nonconforming and mixed finite element methods for Biot's consolidation model. *Numer. Methods Part. Diff. Equ.* **29** (2013) 1749–1777.
- [66] S.-Y. Yi, Convergence analysis of a new mixed finite element method for Biot's consolidation model. *Numer. Methods Part. Diff. Equ.* **30** (2014) 1189–1210.